Controlled Evaluation of Silver Nanoparticle Dissolution Using Atomic Force Microscopy

Ronald D. Kent

Thesis submitted to the faculty of the Virginia Polytechnic Institute and State University in partial fulfillment of the requirements for the degree of

Master of Science
In
Civil Engineering

Peter J. Vikesland, Chair
Andrea M. Dietrich
Linsey C. Marr

November 8, 2011
Blacksburg, VA

Controlled Evaluation of Silver Nanoparticle Dissolution Using Atomic Force Microscopy

Ronald D. Kent

ABSTRACT

Incorporation of silver nanoparticles (AgNPs) into an increasing number of consumer products has led to concern over the potential ecological impacts of their unintended release to the environment. Dissolution is an important environmental transformation that affects the form and concentration of AgNPs in natural waters; however, studies on AgNP dissolution kinetics are complicated by nanoparticle aggregation. Herein, nanosphere lithography (NSL) was used to fabricate uniform arrays of AgNPs immobilized on glass substrates. Nanoparticle immobilization enabled controlled evaluation of AgNP dissolution in an air-saturated phosphate buffer (pH 7, 25 °C) under variable NaCl concentrations in the absence of aggregation. Atomic force microscopy (AFM) was used to monitor changes in particle morphology and dissolution. Over the first day of exposure to ≥10 mM NaCl, the in-plane AgNP shape changed from triangular to circular, the sidewalls steepened, and the height increased by 6-12 nm. Subsequently, particle height and in-plane radius decreased at a constant rate over a 2-week period. Dissolution rates varied linearly from 0.4 to 2.2 nm/d over the 10-550 mM NaCl concentration range tested. NaCl-catalyzed dissolution of AgNPs may play an important role in AgNP fate in saline waters and biological media. This study demonstrates the utility of NSL and AFM for the direct investigation of un-aggregated AgNP dissolution.

Acknowledgements

I also thank my family for their love and support. I could never have received an advanced education without the assistance that my parents, Robert and Linda Kent, have provided to me throughout my life. Also, my wife and daughter, Katie and Hannah Kent, have been a continual source of strength to me. They constantly uplift me and motivate me to be better. Their influence on me has helped me to achieve many of my goals and progress toward others.

Table of Contents

List of Figures

List of Tables

1   Introduction

1.1   OVERVIEW

Silver nanoparticles (AgNPs) are an emerging contaminant that are of concern because of their potential ecotoxicity.[1,2] To mitigate the risks of AgNP release, their environmental transformations must be understood. Dissolution is one of the key processes that will impact the fate of AgNPs in the environment. Size, shape, surface coating, aggregation state, and solution chemistry could all influence how AgNPs dissolve. Previous studies on the dissolution kinetics of AgNPs have left aggregation uncontrolled, so the confounding effects of aggregation leave a gap in our understanding of AgNP dissolution kinetics.[3-5] The goal of the research presented in this thesis was to enable the controlled evaluation of AgNP dissolution rates in the absence of aggregation. Nanosphere lithography (NSL) was chosen to fabricate regular arrays of immobilized AgNPs, and atomic force microscopy (AFM) was used as the primary method to monitor AgNP dissolution. The primary objective of this thesis was to demonstrate that NSL and AFM could be used to obtain meaningful information about the effect of solution chemistry on AgNP dissolution kinetics. Sodium chloride concentration was chosen as the solution chemistry variable since NaCl is present over a broad range of concentrations in natural waters and its influence on AgNP dissolution kinetics had not been studied previously.

Three chapters follow this introductory chapter. Chapter 2 reviews research on the toxicity, fate, and transport of AgNPs in the environment, with emphasis on AgNP dissolution, and describes aspects of NSL and AFM that are important to the present work. Chapter 3 presents original research using NSL and AFM to study the effects of NaCl concentration on AgNP dissolution without aggregation. The final chapter summarizes the engineering significance of the work performed for this thesis.

1.2   ATTRIBUTION

Ronald D. Kent is the primary author of this thesis. Dr. Peter J. Vikesland is coauthor of the third chapter. He made significant edits to drafts of chapter 3 written by Ronald D. Kent. Dr. Vikesland also made important intellectual contributions to chapter 3 and to this work as a whole.

1.3   REFERENCES

(1) Fabrega, J.; Luoma, S. N.; Tyler, C. R.; Galloway, T. S.; Lead, J. R. Silver nanoparticles: Behaviour and effects in the aquatic environment. *Environ. Int.* **2011**, *37*, 517-531.

(2) Marambio-Jones, C.; Hoek, E. M. V. A review of the antibacterial effects of silver nanomaterials and potential implications for human health and the environment. *J. Nanopart. Res.* **2010**, *12*, 1531–1551.

(3) Liu, J.; Hurt, R. H. Ion release kinetics and particle persistence in aqueous nano-silver colloids. *Environ. Sci. Technol.* **2010**, *44*, 2169–2175.

(4) Zhang, W.; Yao, Y.; Sullivan, N.; Chen, Y. S. Modeling the primary size effects of citrate-coated silver nanoparticles on their ion release kinetics. *Environ. Sci. Technol.* **2011**, *45*, 4422-4428.

(5) Kittler, S.; Greulich, C.; Diendorf, J.; Koller, M.; Epple, M. Toxicity of silver nanoparticles increases during storage because of slow dissolution under release of silver ions. *Chem. Mater.* **2010**, *22*, 4548-4554.

2   Literature Review

2.1   ENGINEERED NANOMATERIALS IN THE ENVIRONMENT

Nanomaterials have been operationally defined as materials with at least one characteristic dimension less than 100 nm.[1] In this size range, materials often develop useful attributes that are distinct from the properties of the bulk material. These unique properties have been exploited by incorporating nanomaterials into a wide variety of commercial products, such as textiles, cosmetics, electronics, pharmaceuticals, sensors, and biomedical equipment. As research on nanomaterials continues its accelerated progress, the number of available consumer goods containing nanomaterials is also expected to grow at an increasing rate.

With the rapid advance of nanomaterials into the marketplace, some concern has arisen over the impact these materials might have on public health and the environment.[1,2] Nanomaterials are expected to be released into the environment during each stage of their life cycle, including production, use, and disposal.[3] For example, nanomaterials included in car tires may be released as the tires wear, or nanomaterials present in textiles may partition into leachate after the textiles have been disposed of in a landfill. The recognition that engineered nanomaterials will enter the environment in potentially large quantities raises questions about how their novel properties will affect the way they behave in the environment and interact with living organisms.[4,5] Although research on the environmental impacts of nanomaterials has lagged behind other fields of nanomaterial research, this area is beginning to gain momentum as more studies are investigating the environmental fate, transport, and toxicity of a variety of nanomaterials.

One nanomaterial that is used in a broad range of merchandise is silver nanoparticles (AgNPs). Although they have many useful optical, physical, and chemical properties, it is largely

due to their biocidal effects that AgNPs are included in a variety of commercial products, including such common items as textiles, plastics, soaps, metal products, and pastes.[6] Because AgNPs are included in a large number of everyday items and the number is expected to increase, they have been seen as one of the nanomaterials with high potential for release into the environment at elevated levels. In order to adequately assess and mitigate the risks of AgNPs to public health and the environment, toxicity of and exposure to AgNPs and AgNP transformation products must be quantified.

2.2 TOXICITY OF SILVER NANOPARTICLES

A growing body of research has demonstrated the toxic effects of a variety of forms of nanosilver to several species of vertebrates, invertebrates, and prokaryotic and eukaryotic microorganisms, as well as some mammalian cell lines and viruses.[6,7] Many studies have attempted to elucidate the mechanisms of AgNP toxicity and distinguish between the effects of silver ions (Ag^+) and the nanoparticles themselves, but these questions are still not fully answered because of a number of confounding factors that are difficult to control.[8] Nevertheless, it is clear that factors such as dissolution, size, shape, aggregation state, surface coatings, and solution chemistry can all influence the toxicity of AgNPs.[6,7]

2.2.1 Effects of dissolution on AgNP toxicity

The toxicity of Ag^+ is well known, and researchers often attribute the observed toxicity of AgNPs to the release of Ag^+ by oxidative dissolution. Indeed, it has been suggested that AgNPs are similar to a drug delivery system in which the AgNPs transport and deliver the biologically active compound, Ag^+, to a biological target.[9] It has been shown that partially oxidized AgNPs exhibit more pronounced toxic effects than un-oxidized AgNPs.[10-12] Silver ions released from AgNPs can be re-adsorbed to the particle surface,[13,14] and Lok et al. described how this

phenomenon can lead to toxic levels of Ag^+ localized at the surface of partially oxidized AgNPs.[11] Navarro et al. observed that inhibition of photosynthesis in algae by AgNPs could not be explained solely based on the concentration of Ag^+ released by AgNPs into solution; however, they only measured solution-phase Ag^+ and did not account for heightened levels of Ag^+ adsorbed on AgNP surfaces.[15]

2.2.2   Effects of size and shape on AgNP toxicity

Several studies have documented the increase of AgNP toxicity with decreased size, with AgNPs in the size range of about 1-10 nm being the most toxic.[11,16-18] At least part of the increased toxicity may be explained by the enhanced Ag^+ release from smaller particles due to the increased surface area,[9] but other size effects probably play a role as well. For example, Morones et al. observed that smaller particles preferentially adsorbed to the cell membrane and penetrated into the cell interior of microorganisms.[17] Others have confirmed the ability of AgNPs to attach to microbial surfaces and accumulate within bacterial cells.[12,19,20] Another study showed that AgNPs in the size range 5-46 nm were small enough to diffuse through chorion pore canals of zebrafish embryos, which may lead to a stronger toxic effect than what would be observed for particles that are too large to enter the embryos in a similar manner.[21] Furthermore, polystyrene particles in the nanometer size range have been shown to have a longer retention time in the gut of two suspension-feeding bivalves than micron-sized particles, suggesting that smaller particles may have more potential to bioaccumulate than larger particles.[22] Also, the shape of the particle may be important, as triangular nanoplates have shown greater inhibition of *Escherichia coli* than spherical or rod-shaped AgNPs or Ag^+.[23] This shape effect was attributed to the higher number of reactive, high-atom-density {111} facets on the triangular nanoplates as compared to the spheres and the rods.[17,23]

6

2.2.3 Effects of aggregation on AgNP toxicity

Since smaller sizes and specific shapes appear to enhance AgNP toxicity, it seems reasonable to believe that particle aggregation will diminish toxicity by reducing or eliminating size and shape effects. Indeed, in most cases a decrease in nanoparticle toxicity has been observed as the result of aggregation.[11,24] Some possible explanations of this aggregation effect are that the aggregates do not interact with living organisms in the way smaller, individual particles do; aggregation reduces surface area and thus reduces the amount of toxic Ag^+ released or the potential for surface-bound Ag^+ to interact with living organisms; or aggregates settle out of suspension and are no longer bioavailable. In contrast, it has been observed that aggregation actually enhanced nanoparticle uptake by suspension feeding bivalves, showing that in some cases aggregation may increase bioaccumulation and trophic transfer.[22]

2.2.4 Effects of surface coatings on AgNP toxicity

The role of surface coatings is closely related to aggregation and dissolution. Surface coatings are typically used to prevent aggregation. It has been shown that surface coatings can lead to greater AgNP toxicity by decreasing aggregation.[11,24] However, Kvitek et al. found that surface coatings with comparable stabilizing capacities could affect AgNP toxicity differently, indicating that the nature of the nanoparticle/stabilizer interaction can influence toxicity.[24] In some cases, the stabilizing agent may induce toxic effects beyond those exerted by the nanoparticle itself, as has been shown for C_{60} fullerenes treated with THF.[25] Others have observed that a stabilizing layer decreased toxic effects.[12] Lok et al. found that bovine serum albumin (BSA) initially increased stability and allowed AgNPs to exert bactericidal effects, but an excess of BSA in solution blocked the AgNPs' biocidal action.[11] Another study showed that the presence of natural organic matter (NOM), which can potentially coat AgNPs in the

environment, led to a decrease in observed toxic effects.[25] The authors noted that the presence of NOM also decreased the total silver concentration of filtered samples, suggesting that less free Ag^+ was in solution, which may explain the decrease in toxicity. This result agrees with investigations by Liu and Hurt that showed less dissolution of AgNPs in the presence of NOM.[13]

2.2.5 Effects of solution chemistry on AgNP toxicity

Solution chemistry must also be considered when studying the toxicity of AgNPs because of its dominant role in determining the ultimate form of silver that organisms will encounter in the environment. For example, AgNPs are more likely to be found as aggregates in high ionic strength media.[1,25,26] Also, NOM and ligands present in solution may chelate free Ag^+, chemically reduce Ag^+ to Ag^0, cause Ag^+ to precipitate in one of its many insoluble complexed forms (such as AgCl or Ag_2S), or alter the reactivity of AgNPs by adsorbing to their surfaces.[7,9,11-13,15,25] Often it is assumed that ligand bound metal ions are not bioavailable, but it has been demonstrated that Ag^+ bound by cysteine and glutathione are bioavailable and more toxic than free Ag^+ when reproductive effects to *Ceriodaphnia dubia* are considered rather than mortality.[27]

2.3 EXPOSURE TO SILVER NANOPARTICLES

The results considered in the previous section indicate that AgNPs are toxic to a number of organisms, and heightened release of AgNPs to the environment has potential for negative ecological impacts. It was also emphasized that dissolution, aggregation, and adsorption are all key processes that affect the toxicity of AgNPs. Assessing the potential risk of the release of AgNPs to the environment requires that exposure be accounted for in addition to toxicity.[2,28] Not only must realistic concentrations of AgNPs be predicted for various environmental compartments, but the most likely forms of nanosilver in those compartments must also be

determined. In order to fully account for exposure risks, much more data is needed about the release, transport, and fate of AgNPs in the environment.[3,28-30]

2.3.1   Release of AgNPs to the environment

Studies aimed at quantifying AgNP release during washing of textiles have revealed that significant amounts of silver are released from commercially available fabrics both in the ionic and particulate form, with the specific amount of silver released varying with the manufacturing process and the washing conditions.[31,32] These investigations found that AgNP release is largely due to mechanical stress, but the addition of bleaches can also enhance the release of Ag^+ into the wash water because of greater oxidation potential. Silver released from textiles during washing will typically be transported to a wastewater treatment plant (WWTP). Full-scale and bench-scale studies have shown that silver was removed by about 90% in WWTPs, with a small but significant fraction, partially in the form of AgNPs, remaining in the WWTP effluent while the majority partitioned into the sludge.[31,33,34] Although most of the silver was removed, WWTP effluent still had silver concentrations several orders of magnitude higher than typical river water, and it is expected that AgNPs will be relatively concentrated in WWTP effluents.[29,30,34] The results from these studies also suggest that areas where sludge is land applied will have higher than average concentrations of AgNPs in the soil. In fact, Gottschalk et al. predicted that sludge-treated soil would have an annual increase in AgNP concentration that is up to two orders of magnitude higher than what would be expected for other soil.[29]

2.3.2   Effects of aggregation and adsorption on AgNP fate and transport

Once AgNPs have entered the aquatic environment, dissolution and aggregation will both occur to some extent.[26,35,36] Aggregation can influence dissolution, and vice versa.[37] For example, Zhang et al. showed that the oxidation of AgNPs can change their aggregation

9

kinetics.[35] Dissolution is the focus of this work and will be considered in more detail later. At ionic strengths typical of natural waters, nanoparticle aggregation is expected to occur rapidly.[25,26,38] Aggregates may consist solely of AgNPs, but as Klaine et al. point out, it is more likely that nanoparticles will form aggregates with existing natural colloids, which exist in natural waters at much higher concentrations than the predicted concentrations of AgNPs.[1] Aggregation will typically lead to sedimentation, so it is frequently predicted that sediments will be a major sink for AgNPs,[29,30] but turbulence and nanoparticle uptake by aquatic organisms that feed in the sediments may lead to mobilization and resuspension of nanoparticles.[1]

Stabilizing layers may prevent AgNP aggregation and enable them to remain suspended in the water column. AgNPs are usually stabilized by a charged surface coating, such as citrate, that creates an electrostatic barrier to aggregation. According to classic Derjaguin-Landau-Verwey-Overbeek (DLVO) theory, high ion concentrations shield particles from the repulsive electrostatic force and lead to aggregation as attractive van der Waals interactions promote attachment between particles; however, some surface coatings, such as BSA, lead to an additional repulsive term due to a steric mechanism.[37] Some evidence that BSA provides steric stabilization was given in studies that showed that BSA-coated nanoparticles were stable in high ionic strength media and at the isoelectric point of the particles.[11,39,40] One study showed that 10 and 35-nm gold particles coated with BSA were completely stable in a 10% NaCl solution, but larger gold nanoparticles coated with BSA were not.[40] This observation was explained using DLVO theory, which predicts that increased particle size can lead to the formation of a "secondary minimum" (i.e., a second potential energy well) due to attractive forces that extend further into the solution than repulsive forces. In the case of AgNPs, this result means that the smallest and most toxic particles may also be the most stable, even in saline waters. Even if

AgNPs are not intentionally coated with a steric stabilization layer, proteins and other macromolecules could be adsorbed to the nanoparticle surface in natural aquatic systems and provide additional stability.[41,42]

Although adsorption of NOM and biomolecules could enhance colloidal stability of AgNPs in the environment, the opposite could also be true. Some proteins and amino acids have been observed to induce nanoparticle aggregation.[40,43] Extracellular proteins and intracellular substances that have been released from microbes have also been implicated in nanoparticle aggregation.[19,44] Also, the presence of NOM has actually been observed to lead to enhanced aggregation of nanoparticles under certain solution conditions, particularly when divalent cation concentrations are high.[41,45] Furthermore, the composition and source of NOM have been shown to affect the degree of stabilization imparted by NOM.[46] Whether stability is enhanced or diminished by NOM, recent results suggest that adsorption of NOM will play an even more critical role in the aggregation kinetics of nanoparticles than the capping agents used in nanomaterial synthesis and preparation.[45]

2.3.3 Concentrations of AgNPs in the environment

Several attempts have been made at risk assessments for AgNPs based on the limited data available. The assumptions in these risk assessments vary greatly. Work by Blaser et al. assumed that silver released from AgNP-containing products was entirely in the form of Ag^+, and that all the silver in the environment would be found either in the ionic form or as silver sulfide complexes.[30] They essentially treated the rise of nanosilver as growth of the existing silver industry (e.g., electroplating, photo laboratories, film production, circuit board production), predicting that nanosilver would account for 15% of the silver released in the European Union by 2010; they did not account for any unique risks associated with AgNPs. Modeling efforts by

Nowack and coworkers, on the other hand, only considered nanosilver in their risk assessments, either neglecting silver dissolution or assuming that dissolved silver was eliminated from the system.[28,29] Mueller and Nowack ignored all environmental transformations, including dissolution, aggregation, and sedimentation.[28] Gottschalk et al. attempted to account for the effects of dissolution and sedimentation on AgNP fate, but they disregarded any other environmental transformations.[29] The authors admitted that they were forced to make these assumptions due to the lack of reliable data, which highlights the need for studies on the environmental transformations of AgNPs. Predicted environmental concentrations in surface waters and WWTP effluents from the modeling efforts discussed here are summarized in Table 2-1. Two of the three studies concluded that realistic predicted environmental concentration to predicted no effect concentration ratios (PEC/PNEC) greater than one are possible for nanosilver, indicating a need for further investigation of the effects of nanosilver in the environment.[29,30]

2.4   SILVER NANOPARTICLE DISSOLUTION

As mentioned previously, dissolution can have tremendous effects on the toxicity, fate, and transport of AgNPs. A fundamental understanding of how AgNPs will dissolve once they have been released from commercial products into natural waters is crucial for determining the impact of AgNPs on public health and the environment. Thermodynamic calculations based on the properties of bulk silver suggest that complete dissolution of AgNPs will be favored at environmentally relevant concentrations in oxygenated waters.[13] Although the thermodynamic properties of nanoparticles differ from those of the bulk material,[47,48] the conclusions based on thermodynamic calculations are still valid since silver metal becomes less thermodynamically

stable as its size decreases.[13,49,50] Thus, the question of AgNP dissolution becomes one of chemical kinetics.

The conversion of particulate Ag^0 to aqueous Ag^+ requires an oxidation reaction. It has been observed numerous times that AgNPs are highly sensitive to air and apparently form a surface silver oxide or silver carbonate layer when exposed to air or aerated water, which may make dissolved oxygen the most relevant oxidant for AgNPs in the environment.[13,14,51-54] Indeed, a steep decrease in the Ag^+ release kinetics of AgNPs has been observed under anaerobic conditions.[13] The overall oxidation reaction for oxidation of Ag^0 by oxygen is[13,35]

$$Ag_n(s) + O_2(aq) + 4H^+ \leftrightarrow Ag_{n-4}(s) + 4Ag^+ + 2H_2O \qquad (2\text{-}1)$$
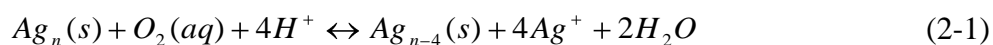
There is some evidence suggesting that the oxidation shown in Equation 2-1 is actually a multi-step process.[9,13] It was proposed that in the first step of the reaction, which was also concluded to be the rate-limiting step, oxygen reacts with silver to form reactive oxygen intermediates that rapidly react with silver in subsequent steps. The overall reaction suggests that pH and the concentrations of dissolved oxygen and AgNPs will all influence the reaction rate.

Although the importance of oxygen as the primary environmental oxidant of AgNPs is stressed here, hydrogen peroxide and other oxidants may be important as well. Dissolution kinetics of AgNPs are much faster in the presence of H_2O_2 than in the presence of oxygen alone.[13,32,55] Some living organisms, such as algae and macrophages, can release H_2O_2 and other reactive oxygen species into solution; thus, interactions between AgNPs and organisms may cause more rapid Ag^+ release than would be predicted based on kinetic models for the oxidation AgNPs by oxygen.[15,55] In fact, one study claimed that algae caused AgNPs to release more Ag^+, which increased the observed toxic effects of AgNPs on the algae.[15] AgNPs may also come into contact with strong oxidants in washing machines.[32] Also, since strong oxidants are frequently

used to disinfect wastewater, AgNPs may encounter high concentrations of oxidants other than oxygen as they pass through WWTPs.

Several groups have researched AgNP reaction rates, and attempts have been made to develop rate laws to predict AgNP dissolution in terms of pH, temperature, AgNP concentration, oxidant availability, and particle size.[10,13,35,55] All of these attempts have arrived at rate laws that are pseudo-first-order in silver concentration. Results from Liu and Hurt suggested that AgNPs may persist in the environment in their colloidal form for only weeks to months.[13] Mass-based dissolution rate constants found in the literature range from 0.01 to 1.5 d^{-1} under various conditions.[10,13,35]

Although these studies are a necessary and good first step to understanding AgNP dissolution, most of the experiments were performed in environmentally irrelevant solutions, such as deionized water, or at environmentally unrealistic concentrations (e.g., on the order of µg/L to mg/L instead of the predicted ng/L concentrations given in Table 2-1). Also, the possible confounding effects of aggregation were uncontrolled in all cases. In order to arrive at a more complete view of how AgNP dissolution will occur in the environment, an experimental setup that allows precise control over nanoparticle size, shape, and aggregation as well as environmental factors (such as pH and ionic strength) is needed.

2.4.1 Effects of size, shape, and crystallinity on AgNP dissolution

Numerous studies have shown that smaller AgNPs dissolve more rapidly than large ones.[8,9,35,54,55] This result is partially explained by the larger surface area of smaller particles on an equivalent mass basis; if more surface atoms are exposed, then more reaction sites are available for oxidation and subsequent dissolution.[9] However, normalizing dissolution rates by surface area cannot fully account for the size-dependent dissolution of nanoparticles.[50,56]

14

Theoretical and experimental work has shown that as particle size decreases, redox potential becomes more negative, which means that small particles will be more readily oxidized and will be less thermodynamically stable than larger particles of the same material.[49,50,57] This decrease in redox potential has been related to the increase in surface free energy that occurs as surface area increases.[47,57] The enhanced reactivity of nanomaterials can also be attributed to their large number of edges, corners, and high energy surface defects.[10,35,50] Nanoparticles also tend to present a higher number of reactive {111} facets than larger particles.[17,50]

Shape and crystallinity may also affect AgNP dissolution rates. For example, it may be predicted that triangular silver nanoplates will dissolve more rapidly than silver nanospheres or nanorods because of their allegedly higher concentration of exposed {111} facets, which may partially explain their enhanced toxicity.[23] Additionally, nonspherical AgNPs have been observed to dissolve preferentially at locations with a small radius of curvature;[58] therefore, AgNPs with shapes containing numerous sharp edges and corners are expected to release Ag^+ more rapidly than smoother particles. Studies have also provided evidence that polycrystalline AgNPs will dissolve more rapidly than single-crystalline AgNPs.[59-61] The proposed explanation for this behavior is that polycrystalline particles contain high-energy defects at grain boundaries that provide active sites for oxidation and dissolution.

2.4.2 Effects of pH, temperature, and ionic strength on AgNP dissolution

From Equation 2-1, AgNPs would be expected to dissolve more rapidly at low pH. Proposed kinetic models also predict that lower pH will lead to faster dissolution kinetics.[13,35] These predictions agree with experimental data that showed an approximately six-fold increase of one-day Ag^+ release when pH was decreased from 8 to 4.[13] On the other hand, dissolution rates increased with increasing pH in a study where hydrogen peroxide was used as the primary

oxidant instead of oxygen.[55] This observation is probably due to the dissociation of H_2O_2 at high pH to form the hydroperoxide anion, HO_2^-, which is expected to have a stronger interaction with the silver surface since it is a stronger nucleophile than the undissociated form.[62] This result may be important for conditions that are relevant to textile washing where pH may be high and H_2O_2 may be present in bleach.[32]

Kinetic models for AgNP dissolution that include temperature effects predict that the reaction will proceed more rapidly at elevated temperatures.[13,35] Again, experimental data have confirmed this trend.[10,13,55] Kittler et al. observed that during a 200-h period, dissolution of 0.1 g/L 50-nm PVP-coated AgNPs as percent of the initial silver mass varied from about 5% at 5 °C to about 50% at 25 °C to about 90% at 37 °C.[10] The proposed kinetic models do not include ionic strength, but ionic strength could affect the dissolution rate of AgNPs by reducing the solubility of oxygen or by causing aggregation.[35] Specific ions that contribute to ionic strength, such as chloride, may also have a strong influence on AgNP dissolution kinetics. In the case of hydrogen peroxide, ionic strength did not appear to have any effect on AgNP dissolution.[55] It is evident from data presented by Liu and Hurt that ionic strength had some influence on the reaction kinetics, probably mostly due to aggregation, but the authors dismissed this effect as minor compared to the influence of pH.[13]

2.4.3 Effects of ligands and surface coating on AgNP dissolution

A number of researchers have observed that ligands catalyzed the oxidation of AgNPs, and this effect was more pronounced for stronger nucleophiles.[36,53,59,60,63-68] Henglein and coworkers, who pioneered work on the interactions between ligands and AgNPs, explained this observation by postulating that a "pre-complexation" or "pre-oxidation" occurred when nucleophiles adsorbed to the nanoparticle surface.[65-67] According to their hypothesis, the

16

coordination of a nucleophile to a surface silver atom results in the partial oxidation of that atom. The excess electron density is accepted by the particle interior and imparts a more negative redox potential to the AgNP, and thus lowers the free energy barrier to oxidation. The presence of an electron acceptor, such as O_2, drives the oxidation to completion by removing the excess electron density from the particle interior and releasing the silver-ligand complex into solution.

Not only did Henglein and coworkers observe that stronger nucleophiles caused more rapid dissolution of AgNPs than weak ones, they also observed that ligands that interact more strongly with silver will displace ligands that experience weaker interactions with silver.[65,69,70] This result indicates that stabilizing agents that are weakly complexed to AgNP surfaces, such as citrate, may be rapidly displaced by ligands in the natural environment. In fact, Levard et al. observed that aqueous sulfides would displace PVP surface coatings from AgNPs.[71] It may also be inferred from this result that strong nucleophiles will play a dominant role in AgNP dissolution rates in the environment. Inorganic and organic sulfides form stronger bonds with silver than perhaps any other ligand that AgNPs will commonly encounter in the environment.[65,70,72] Somewhat counterintuitively, inorganic and organic sulfides have been measured in a number of oxic waters.[72-75] Even though sulfides might be expected to be rapidly oxidized in freshwater, some of the concentrations measured are actually about two orders of magnitude higher than measured silver concentrations in oxygenated waters.[73] Therefore, sulfides are expected to largely control dissolution of AgNPs in freshwater environments. This conclusion is corroborated by a study that identified Ag_2S nanoparticles in the effluent of full-scale WWTPs.[76] In marine environments, chloride may be the principal ligand influencing AgNP dissolution.

Although ligands can accelerate AgNP dissolution, they will not necessarily promote the release of Ag^+ into aqueous solutions. In fact, the opposite has been observed in several cases.[9,71,77] If the ligand-Ag^+ complex is insoluble, then a precipitate may form. For example, Henglein et al. spectrophotometrically measured the formation of Ag_2S colloids upon dissolution of AgNPs in the presence of HS^- and O_2.[65] The precipitate can also form a passivating layer on AgNP surfaces and prevent further dissolution. This phenomenon has been observed or implicated for sulfide, bromide, and chloride.[9,26,55,71] For AgNPs in contact with air, corrosion induced by atmospheric sulfides caused an Ag_2S shell to form on the nanoparticles.[61] Levard et al. found that sulfidation of AgNPs in solution led to the formation of Ag_2S bridges between nanoparticles by a dissolution/precipitation mechanism.[71] They also observed that the amount of Ag_2S present on AgNPs increased as the S/Ag ratio increased. For S/Ag > 1, metallic silver was no longer detectable by X-ray diffraction. In their study, the presence of Ag_2S on the AgNPs decreased the amount of detectable dissolved silver species.

Cysteine, other thiol-containing compounds, and NOM have also been observed to decrease soluble silver concentrations, even when cysteine is added to Ag^+ solutions rather than AgNP suspensions.[9,13,15,25,77] Some silver-thiol complexes, including silver cysteinate, are sparingly soluble, so precipitation could partially explain these results.[78] Even when such complexes are soluble, they have been observed to exist in solution as aggregates, so in some cases they may be removed by filtration steps preceding soluble silver measurements.[72] Also, one study provided evidence for the removal of Ag^+ from solution by the reduction of Ag^+ to metallic silver by cysteine and thiosulfate.[77] Another commonly employed explanation is that surface-bound ligands compete with O_2 for surface sites and thus decrease the rate of oxidation. Liu et al. provided evidence for this mechanism by demonstrating that Ag^+ release from AgNPs

was diminished as citrate surface coatings became more densely-packed.[9] In a control experiment, they demonstrated that the observed effect was not due to reduction of Ag^+ to metallic silver by citrate. Differences in surface coverage may explain why Kittler et al. observed more rapid dissolution for PVP-coated AgNPs than citrate-coated AgNPs whereas Ho et al. observed a decrease in the dissolution rates of citrate-coated AgNPs when PVP was added.[10,55] Finally, if reactive oxygen intermediates are formed during the oxidation of AgNPs, then dissolution may be hindered by scavenging of these reactive intermediates by organic compounds, such as NOM.[9,13]

2.4.4 Effects of aggregation on AgNP dissolution

Because dissolution and aggregation of AgNPs occur simultaneously, almost every study that discusses one of these processes of necessity addresses the other as well.[13,26,35,36,54,79] The influence of aggregation on nanomaterial reactivity has been observed in several cases.[37] Experimental evidence indicates that aggregation quenches dissolution rates of goethite nanorods and galena nanoparticles by an order of magnitude or more.[50,80] Production of reactive oxygen species (ROS) by C_{60} fullerenes can also be diminished by particle aggregation.[81,82] Oxidation of nanoparticulate magnetite by carbon tetrachloride has been demonstrated to decrease in conditions that favor aggregation.[56] Aggregation has also been implicated in reduced reactivity of amorphous ferric oxyhydroxides.[83] Zhang et al. found that aggregation reduced the correlation between a pseudo-first-order kinetic model and experimental results as time elapsed.[35]

The observed decrease in nanomaterial reactivity with aggregation in most of these cases can probably be explained by two mechanisms. First, as particles attach to each other during aggregation the total surface area exposed to the solution will decrease, so the number of sites available for reaction will also decrease. Also, constrained aggregate structures can lead to

decreased rates of mass transfer, so reactants will be transported to reaction sites more slowly than they would if the nanomaterials were well dispersed.[50,56] In the case of C_{60} fullerenes, decreased photochemical ROS production may have been due to self-quenching resulting from the close particle contact conditions that exist within a tight aggregate structure.[37] A model developed by Hotze et al. predicts that nanoparticle reactivity will decrease, possibly by orders of magnitude, as aggregates grow larger and as their structure becomes more closed.[82] Since solution chemistry, particle shape, particle size, and surface functionalization can all play a large role in the size and structure of aggregates,[37] conclusions about the effects any of these factors may have on AgNP dissolution can be confounded by particle aggregation. Clearly, arriving at a correct understanding of how a variety of parameters affect AgNP dissolution requires that experiments be performed in the absence of the confounding effects of aggregation.

2.5   CONTROLLED SILVER NANOPARTICLE DISSOLUTION EXPERIMENTS

Several researchers have recognized the effects aggregation can have on reactivity and have attempted to experimentally separate the influence of aggregation. One common approach to resolve this problem is to vary experimental conditions in a manner that attempts to distinguish between the influence of the solution chemistry and aggregation.[56,80] The difficulty with this method is that the influence of aggregation is never actually uncoupled from the specific solution conditions under which aggregation occurs. Another technique is to attach nanoparticles to a substrate.[8,50,51] In this case, aggregation cannot occur because the particles are immobilized. Studies using this method have focused on attaching pre-formed colloidal particles to substrates.[50,51] Using lithographic techniques that allow nanostructures to be fabricated directly on substrates would provide an additional level of control.

A variety of lithographic techniques are available to precisely control shape and size at the nanoscale. In the most extreme case, atom-by-atom or molecule-by-molecule construction is possible for some materials using scanning probe technology.[84,85] In spite of the unprecedented control offered by scanning probe techniques, they are inherently low-throughput, which limits their applicability.[86] Electron- and ion-beam lithography offer high resolution control of features, but these methods are also low-throughput and expensive.[86-88] Photolithography is a high-throughput and relatively inexpensive method that allows the controlled fabrication of patterned structures, but objects that are created by photolithography can be no smaller than the diffraction limit of the optical device used during the exposure step.[89] Efforts to overcome this restraint include reaching further into the ultraviolet light range or using X-ray lithography.[87,89] For the purposes of this study, nanosphere lithography (NSL) has been chosen since it is a versatile, inexpensive, and high-throughput lithographic technique.[86]

2.5.1   Nanosphere lithography

The key feature of NSL is the self-assembly of a patterned mask of colloidal particles on a substrate followed by the deposition of a material over the mask to produce a periodic particle array.[86] The self-assembly is accomplished simply by depositing a colloidal suspension on a substrate and allowing the solvent to evaporate. In this step, suspensions of latex spheres may be deposited by a number of simple methods, including drop-casting,[90] spin-coating,[91] or convective self-assembly.[92] As the solvent evaporates, the suspended spheres are pulled together by capillary forces to form a hexagonally close-packed monolayer or bilayer.[93] In order for the self-assembly step to occur spontaneously, the colloids must have the same charge as the substrate so that they do not attach to the substrate in a random fashion, and the substrate must be hydrophilic.[86] The final mask fabricated in this way always includes a number of crystal defects;

however, colloidal masks can be assembled using other similar techniques, such as dip-coating, that reduce defect concentrations, but these alternate strategies are rarely as fast or simple as the process described here.[94,95] Once the mask is ready, a material, usually a metal, is deposited onto the substrate through the mask. Thermal evaporation is the most common method for this deposition step.[86] Finally, the colloidal mask is removed to reveal the resultant periodic particle array.

Fischer and Zingsheim were the first to employ this technique.[90] They deposited the colloidal mask simply by drop-casting a suspension of latex spheres onto the substrate. Platinum was vacuum deposited on top of the mask to create a pattern that was further processed and used for contact imaging. Deckman and co-workers researched this process more in-depth and coined the term "natural lithography" to highlight the self-assembly of the spherical colloids into a crystalline mask.[91,96,97] Rather than drop-casting the suspension onto a substrate, they deposited the latex spheres by spin-coating, which allowed them to cover larger areas with the mask. They also enumerated possible applications for this lithographic technique, including surface enhanced Raman scattering, photovoltaics, and formation of optical elements. Van Duyne and co-workers changed the name of natural lithography to nanosphere lithography and further extended its use by exploring new options for controlling and characterizing the size, shape, and interparticle spacing of the periodic particle arrays produced by NSL.[93] Their work has demonstrated the control and versatility offered by NSL and the utility of NSL for fundamental studies of nanomaterial properties.[86,93]

NSL provides control over nanoparticle size, shape, and interparticle spacing. Particle height is adjusted by varying the duration of the metal evaporation while lateral dimensions and interparticle spacing are controlled by varying the size of the colloidal particles used for creating

the mask.[98] A simple monolayer mask will yield particles with a truncated tetrahedral shape and a bilayer mask will result in hexagonal particles.[93] Even more control over lateral dimensions, interparticle spacing, and particle shape can be achieved by varying the angle of the substrate relative to the direction of the material deposition beam.[86,99] Particle morphology can also be controlled by additional processing of the particle array. For example, truncated tetrahedral particles have been converted into hemispherical particles by electrochemical and thermal processing.[58,100] Alternatively, the mask itself can be etched to produce a variety of complex shapes and patterns.[94,101]

Another advantage of NSL is that it is considered to be a materials-general lithographic technique. In their initial work, Hulteen and Van Duyne showed that several different substrates (e.g., mica, glass, silicon, gold, copper) and deposition materials (e.g., silver, gold, chromium, calcium fluoride, cobalt phthalocyanine) could be used for NSL.[93] Since a variety of substrates can be used, nanomaterial properties can be tested on several different substrates to test how the substrate itself might affect the properties that are being evaluated.[102] Furthermore, NSL has been used to create templates for the directed growth or attachment of other materials. For example, periodic arrays of quantum dots,[103] aligned carbon nanotubes,[104] and aligned zinc oxide nanorods[105] have all been produced using templates fabricated by NSL. Thus, numerous nanomaterials may be precisely fabricated by NSL for controlled studies of their unique properties. In particular, NSL can be used by environmental engineers and scientists as a tool for fundamental evaluations of how nanomaterial morphology will influence nanomaterial behavior during important environmental processes, such as dissolution, oxidation, and adsorption.

2.5.2 Measuring dissolution by atomic force microscopy

Atomic force microscopy (AFM) is an obvious choice for characterizing dissolutive changes in the size and shape of NSL-produced AgNPs since it can resolve sample topography with sub-nanometer precision. By taking before-and-after AFM micrographs, Zhang et al. were able to demonstrate that the truncated tetrahedral AgNPs produced by NSL were preferentially oxidized along their edges during an electrochemical process.[58] Hasse and Scholz used AFM to observe the electrochemical conversion of an individual silver sulfide particle to silver metal and to measure the associated volume reduction.[106] Another advantage of AFM is that it can be used with a fluid cell, with or without flow, to track morphologic changes of particles *in situ*. This technique has been successfully employed to study the development of pit morphologies during calcite dissolution.[107,108]

Although AFM is capable of performing high-resolution topographic scans *in situ*, it suffers from tip-induced artifacts. Because AFM relies on a probe with a definite size and shape for measurements, AFM images represent a convolution of the sample and tip geometries. Particle height information is unaffected by this convolution, but measured lateral particle dimensions are always greater than the true sample dimensions. This effect is more pronounced when particle dimensions are comparable to the radius of curvature of the AFM tip. Moreover, the fixed aspect ratio of AFM probes prevents the correct interpretation of steep sample features. For example, if an AFM probe has a 45° sidewall angle, then all sample features steeper than 45° will appear to have a 45° incline. Hence, obtaining quantitative information about lateral dimensions from AFM data requires a deconvolution procedure.

To appropriately perform a deconvolution of AFM data, something must be known about the tip geometry or the sample geometry. A common practice is to assume that the AFM tip is a

sphere, a parabola, or another simple geometric shape.[109,110] Once such an assumption has been made, geometric parameters, such as the radius of curvature, must be measured or estimated. Authors will frequently assume a radius of curvature based on nominal values.[111,112] The radius of curvature can be measured indirectly by using latex spheres or gold nanoparticles as a calibration standard.[113,114] After the geometric description of the probe is complete, a mathematical treatment of the data, typically using Legendre transforms, is performed to reconstruct the sample geometry.[109,110] Alternatively, a numerical approach proposed by Markiewicz and Goh can be used to reconstruct the tip geometry from a known sample geometry or to reconstruct the sample geometry from known tip geometry.[115] Their procedure utilizes the fact that each data point represents the position of the probe's apex. A facsimile of the probe is placed at each data point, and surrounding data points that are in conflict with the tip geometry are altered so that their new height is no longer in conflict with the tip geometry. On the other hand, if a known sample geometry is placed at each point, then this deconvolution procedure will yield a description of the tip geometry.

While the deconvolution methods described here can reduce errors caused by tip effects, they cannot give information about areas that are inaccessible to the AFM probe.[109,115] Also, any assumptions made about tip geometry will result in inaccuracies in the reconstructed sample data. Furthermore, even if the tip geometry is measured carefully, the geometry can change during a scan if the tip becomes contaminated or dull, and using calibration standards to measure the tip radius every time the AFM probe is replaced can be tedious or impractical. Thus, comparison with other techniques, such as scanning or transmission electron microscopy, is necessary to arrive at a more accurate description of the true sample geometry. UV-Vis absorption data can be correlated with morphological changes of AgNPs measured by AFM.[58]

As has been done in the case of calcite, aqueous-phase methods can also complement dissolution information obtained by AFM.[107,108] For example, inductively coupled plasma mass spectrometry (ICP-MS) can be used as a sensitive technique for measuring Ag^+ concentrations in solutions that have been used for AFM-based AgNP dissolution experiments. Spectroscopic methods, such as X-ray photoelectron spectroscopy (XPS), Raman spectroscopy, and energy dispersive spectroscopy (EDS), can provide additional information about chemical changes that occur in AgNPs during the dissolution process.

2.6   CONCLUSION

As the number of commercial products containing AgNPs increases, the level of AgNPs in the environment will increase as well. In order to evaluate how AgNPs will affect human health and the environment, the toxicity of and potential for exposure to these nanomaterials must be well understood. A growing body of research has demonstrated that AgNPs can exert toxic effects on a variety of living organisms and that these toxic effects depend on numerous variables, including particle size, shape, surface coating, and aggregation state. Also, initial risk assessment efforts indicate that AgNPs may enter the environment at concentrations that will have negative ecological impacts, but information about the environmental transformations of AgNPs is still lacking.

Dissolution and aggregation are both important processes affecting the toxicity, fate, and transport of AgNPs. These two processes occur simultaneously, and they can each influence how the other proceeds. Gaining a fundamental understanding of how particle properties (e.g., size, shape, surface coating) and solution chemistry impact dissolution and aggregation requires that each process be studied independently of the other. If AgNPs are firmly attached to a substrate, then they will not be able to aggregate, so their dissolution behavior may be studied directly.

Regular arrays of AgNPs with controlled shape and size can be fabricated directly on substrates by NSL. Changes in the size and shape of the AgNPs produced by NSL can be characterized by AFM and correlated with other complementary techniques. In this manner, a detailed view of AgNP dissolution as a function of particle size, shape, surface coating, and solution chemistry can be obtained, which will lead to a greater understanding of how AgNPs will be transformed once they enter aquatic environments. This understanding is essential for the success of future efforts to assess and mitigate risks related to the release of AgNPs into the environment.

2.7   REFERENCES

(1) Klaine, S. J.; Alvarez, P. J. J.; Batley, G. E.; Fernandes, T. F.; Handy, R. D.; Lyon, D. Y.; Mahendra, S.; Mclaughlin, M. J.; Lead, J. R. Nanomaterials in the environment: Behavior, fate, bioavailability, and effects. *Environ. Toxicol. Chem.* **2008**, *27*, 1825-1851.

(2) Wiesner, M. R.; Lowry, G. V.; Alvarez, P.; Dionysiou, D.; Biswas, P. Assessing the risks of manufactured nanomaterials. *Environ. Sci. Technol.* **2006**, *40*, 4336-4345

(3) Gottschalk, F.; Nowack, B. The release of engineered nanomaterials to the environment. *J. Environ. Monit.* **2011**, *13*, 1145-1155.

(4) Nel, A. E.; Madler, L.; Velegol, D.; Xia, T.; Hoek, E. M. V.; Somasundaran, P.; Klaessig, F.; Castranova, V.; Thompson, M. Understanding biophysicochemical interactions at the nano-bio interface. *Nat. Mater.* **2009**, *8*, 543-557.

(5) Nel, A.; Xia, T.; Madler, L.; Li, N. Toxic potential of materials at the nanolevel. *Science* **2006**, *311*, 622-627.

(6) Fabrega, J.; Luoma, S. N.; Tyler, C. R.; Galloway, T. S.; Lead, J. R. Silver nanoparticles: Behaviour and effects in the aquatic environment. *Environ. Int.* **2011**, *37*, 517-531.

(7) Marambio-Jones, C.; Hoek, E. M. V. A review of the antibacterial effects of silver nanomaterials and potential implications for human health and the environment. *J. Nanopart. Res.* **2010**, *12*, 1531–1551.

(8) Sotiriou, G. A.; Pratsinis, S. E. Antibacterial activity of nanosilver ions and particles. *Environ. Sci. Technol.* **2010**, *44*, 5649-5654.

(9) Liu, J.; Sonshine, D. A.; Shervani, S.; Hurt, R. H. Controlled release of biologically active silver from nanosilver surfaces. *ACS Nano* **2010**, *4*, 6903–6913.

(10) Kittler, S.; Greulich, C.; Diendorf, J.; Koller, M.; Epple, M. Toxicity of silver nanoparticles increases during storage because of slow dissolution under release of silver ions. *Chem. Mater.* **2010**, *22*, 4548-4554.

(11) Lok, C.; Ho, C.; Chen, R.; He, Q.; Yu, W.; Sun, H.; Tam, P.; Chiu, J.; Che, C. Silver nanoparticles: Partial oxidation and antibacterial activities. *J. Biol. Inorg. Chem.* **2007**, *12*, 527-534.

(12) Smetana, A. B.; Klabunde, K. J.; Marchin, G. R.; Sorensen, C. M. Biocidal activity of nanocrystalline silver powders and particles. *Langmuir* **2008**, *24*, 7457-7464.

(13) Liu, J.; Hurt, R. H. Ion release kinetics and particle persistence in aqueous nano-silver colloids. *Environ. Sci. Technol.* **2010**, *44*, 2169–2175.

(14) Henglein, A. Colloidal silver nanoparticles: Photochemical preparation and interaction with O_2, CCl_4, and some metal ions. *Chem. Mater.* **1998**, *10*, 444-450.

(15) Navarro, E.; Piccapietra, F.; Wagner, B.; Marconi, F.; Kaegi, R.; Odzak, N.; Sigg, L.; Behra, R. Toxicity of silver nanoparticles to *Chlamydomonas Reinhardtii*. *Environ. Sci. Technol.* **2008**, *42*, 8959-8964.

(16) Choi, O.; Hu, Z. Q. Size dependent and reactive oxygen species related nanosilver toxicity to nitrifying bacteria. *Environ. Sci. Technol.* **2008**, *42*, 4583-4588.

(17) Morones, J. R.; Elechiguerra, J. L.; Camacho, A.; Holt, K.; Kouri, J. B.; Ramirez, J. T.; Yacaman, M. J. The bactericidal effect of silver nanoparticles. *Nanotechnology* **2005**, *16*, 2346-2353.

(18) Elechiguerra, J. L.; Burt, J. L.; Morones, J. R.; Camacho-Bragado, A.; Gao, X.; Lara, H. H.; Yacaman, M. J. Interaction of silver nanoparticles with HIV-1. *J. Nanobiotechnology* **2005**, *3*, 6-15.

(19) Sondi, I.; Salopek-Sondi, B. Silver nanoparticles as antimicrobial agent: A case study on *E-Coli* as a model for gram-negative bacteria. *J. Colloid Interface Sci.* **2004**, *275*, 177-182.

(20) Choi, O.; Deng, K. K.; Kim, N.; Jr., L. R.; Surampalli, R. Y.; Hu, Z. The inhibitory effects of silver nanoparticles, silver ions, and silver chloride colloids on microbial growth. *Water Res.* **2008**, *42*, 3066-3074.

(21) Lee, K. J.; Nallathamby, P. D.; Browning, L. M.; Osgood, C. J.; Xu, X. H. N. *In vivo* imaging of transport and biocompatibility of single silver nanoparticles in early development of zebrafish embryos. *ACS Nano* **2007**, *1*, 133-143.

(22) Ward, J. E.; Kach, D. J. Marine aggregates facilitate ingestion of nanoparticles by suspension-feeding bivalves. *Mar. Environ. Res.* **2009**, *68*, 137-142.

(23) Pal, S.; Tak, Y. K.; Song, J. M. Does the antibacterial activity of silver nanoparticles depend on the shape of the nanoparticle? A study of the gram-negative bacterium *Escherichia Coli*. *Appl. Environ. Microbiol.* **2007**, *73*, 1712-1720.

(24) Kvitek, L.; Panacek, A.; Soukupova, J.; Kolar, M.; Vecerova, R.; Prucek, R.; Holecova, M.; Zboril, R. Effect of surfactants and polymers on stability and antibacterial activity of silver nanoparticles (nps). *J. Phys. Chem. C* **2008**, *112*, 5825-5834.

(25) Gao, J.; Youn, S.; Hovsepyan, A.; Llaneza, V. L.; Wang, Y.; Bitton, G.; Bonzongo, J. C. J. Dispersion and toxicity of selected manufactured nanomaterials in natural river water samples: Effects of water chemical composition. *Environ. Sci. Technol.* **2009**, *43*, 3322-3328.

(26) Li, X.; Lenhart, J. J.; Walker, H. W. Dissolution-accompanied aggregation kinetics of silver nanoparticles. *Langmuir* **2010**, *26*, 16690-16698.

(27) Bielmyer, G. K.; Bell, R. A.; Klaine, S. J. Effects of ligand-bound silver on *Ceriodaphnia Dubia*. *Environ. Toxicol. Chem.* **2002**, *21*, 2204-2208.

(28) Mueller, N. C.; Nowack, B. Exposure modeling of engineered nanoparticles in the environment. *Environ. Sci. Technol.* **2008**, *42*, 4447-4453.

(29) Gottschalk, F.; Sonderer, T.; Scholz, R. W.; Nowack, B. Modeled environmental concentrations of engineered nanomaterials (TiO_2, ZnO, Ag, CNT, fullerenes) for different regions. *Environ. Sci. Technol.* **2009**, *43*, 9216-9222.

(30) Blaser, S. A.; Scheringer, M.; Macleod, M.; Hungerbühler, K. Estimation of cumulative aquatic exposure and risk due to silver: Contribution of nano-functionalized plastics and textiles. *Sci. Total Environ.* **2008**, *390*, 396–409.

(31) Benn, T. M.; Westerhoff, P. Nanoparticle silver released into water from commercially available sock fabrics. *Environ. Sci. Technol.* **2008**, *42*, 4133–4139.

(32) Geranio, L.; Heuberger, M.; Nowack, B. The behavior of silver nanotextiles during washing. *Environ. Sci. Technol.* **2009**, *43*, 8113–8118.

(33) Tiede, K.; Boxall, A. B. A.; Wang, X.; Gore, D.; Tiede, D.; Baxter, M.; David, H.; Teare, S. P.; Lewis, J. Application of hydrodynamic chromatography-ICP-MS to investigate the fate of silver nanoparticles in activated sludge. *J. Anal. At. Spectrom.* **2010**, *25*, 1149–1154.

(34) Shafer, M. M.; Overdier, J. T.; Armstong, D. E. Removal, partitioning, and fate of silver and other metals in wastewater treatment plants and effluent-receiving streams. *Environ. Toxicol. Chem.* **1998**, *17*, 630-641.

(35) Zhang, W.; Yao, Y.; Sullivan, N.; Chen, Y. S. Modeling the primary size effects of citrate-coated silver nanoparticles on their ion release kinetics. *Environ. Sci. Technol.* **2011**, *45*, 4422-4428.

(36) Hsu-Kim, H.; Gondikas, A.; Deonarine, A.; Masion, A.; Auffan, M. Sorption of natural organic ligands to silver and zinc sulfide nanoparticles: Implications for aggregation and dissolution. *Geochim. Cosmochim. Acta* **2010**, *74*, A422-A422.

(37) Hotze, E. M.; Phenrat, T.; Lowry, G. V. Nanoparticle aggregation: Challenges to understanding transport and reactivity in the environment. *J. Environ. Qual.* **2010**, *39*, 1909-1924.

(38) Trinh, L. T. T.; Kjoniksen, A. L.; Zhu, K. Z.; Knudsen, K. D.; Volden, S.; Glomm, W. R.; Nystrom, B. Slow salt-induced aggregation of citrate-covered silver particles in aqueous solutions of cellulose derivatives. *Colloid Polym. Sci.* **2009**, *287*, 1391-1404.

(39) Brewer, S. H.; Glomm, W. R.; Johnson, M. C.; Knag, M. K.; Franzen, S. Probing BSA binding to citrate-coated gold nanoparticles and surfaces. *Langmuir* **2005**, *21*, 9303-9307.

(40) Yoo, E. J.; Li, T.; Park, H. G.; Chang, Y. K. Size-dependent flocculation behavior of colloidal Au nanoparticles modified with various biomolecules. *Ultramicroscopy* **2008**, *108*, 1273-1277.

(41) Chen, K. L.; Elimelech, M. Influence of humic acid on the aggregation kinetics of fullerene (C-60) nanoparticles in monovalent and divalent electrolyte solutions. *J. Colloid Interface Sci.* **2007**, *309*, 126-134.

(42) Saleh, N. B.; Pfefferle, L. D.; Elimelech, M. Aggregation kinetics of multiwalled carbon nanotubes in aquatic systems: Measurements and environmental implications. *Environ. Sci. Technol.* **2008**, *42*, 7963-7969.

(43) Zhang, D. M.; Neumann, O.; Wang, H.; Yuwono, V. M.; Barhoumi, A.; Perham, M.; Hartgerink, J. D.; Wittung-Stafshede, P.; Halas, N. J. Gold nanoparticles can induce the formation of protein-based aggregates at physiological pH. *Nano Lett.* **2009**, *9*, 666-671.

(44) Moreau, J. W.; Weber, P. K.; Martin, M. C.; Gilbert, B.; Hutcheon, I. D.; Banfield, J. F. Extracellular proteins limit the dispersal of biogenic nanoparticles. *Science* **2007**, *316*, 1600-1603.

(45) Stankus, D. P.; Lohse, S. E.; Hutchison, J. E.; Nason, J. A. Interactions between natural organic matter and gold nanoparticles stabilized with different organic capping agents. *Environ. Sci. Technol.* **2011**, *45*, 3238-3244.

(46) Deonarine, A.; Lau, B. L. T.; Aiken, G. R.; Ryan, J. N.; Hsu-Kim, H. Effects of humic substances on precipitation and aggregation of zinc sulfide nanoparticles. *Environ. Sci. Technol.* **2011**, *45*, 3217-3223.

(47) Luo, W. H.; Hu, W. Y.; Xiao, S. F. Size effect on the thermodynamic properties of silver nanoparticles. *J. Phys. Chem. C* **2008**, *112*, 2359-2369.

(48) Gilbert, B.; Huang, F.; Zhang, H. Z.; Waychunas, G. A.; Banfield, J. F. Nanoparticles: Strained and stiff. *Science* **2004**, *305*, 651-654.

(49) Henglein, A. Small-particle research: Physicochemical properties of extremely small colloidal metal and semiconductor particles. *Chem. Rev.* **1989**, *89*, 1861-1873.

(50) Liu, J.; Aruguete, D. M.; Murayama, M.; Hochella, M. F. Influence of size and aggregation on the reactivity of an environmentally and industrially relevant manomaterial (PbS). *Environ. Sci. Technol.* **2009**, *43*, 8178-8183.

(51) Pallavicini, P.; Taglietti, A.; Dacarro, G.; Diaz-Fernandez, Y. A.; Galli, M.; Grisoli, P.; Patrini, M.; Santucci De Magistris, G.; Zanoni, R. Self-assembled monolayers of silver nanoparticles firmly grafted on glass surfaces: Low Ag^+ release for an efficient antibacterial activity. *J. Colloid Interface Sci.* **2010**, *350*, 110-116.

(52) Yin, Y.; Li, Z.; Zhong, Z.; Gates, B.; Xia, Y.; Venkateswaran, S. Synthesis and characterization of stable aqueous dispersions of silver nanoparticles through the Tollens process. *J. Mater. Chem.* **2002**, *12*, 522–527.

(53) Pal, T.; Sau, T. K.; Jana, N. R. Reversible formation and dissolution of silver nanoparticles in aqueous surfactant media. *Langmuir* **1997**, *13*, 1481-1485.

(54) Elzey, S.; Grassian, V. H. Agglomeration, isolation and dissolution of commercially manufactured silver nanoparticles in aqueous environments. *J. Nanopart. Res.* **2010**, *12*, 1945–1958.

(55) Ho, C.; Yau, S.; Lok, C.; So, M.; Che, C. Oxidative dissolution of silver nanoparticles by biologically relevant oxidants: A kinetic and mechanistic study. *Chem. Asian J.* **2010**, *5*, 285-293.

(56) Vikesland, P. J.; Heathcock, A. M.; Rebodos, R. L.; Makus, K. E. Particle size and aggregation effects on magnetite reactivity toward carbon tetrachloride. *Environ. Sci. Technol.* **2007**, *41*, 5277-5283.

(57) Plieth, W. J. Electrochemical properties of small clusters of metal atoms and their role in surface enhanced Raman scattering. *J. Phys. Chem.* **1982**, *86*, 3166-3170.

(58) Zhang, X.; Hicks, E. M.; Zhao, J.; Schatz, G. C.; Van Duyne, R. P. Electrochemical tuning of silver nanoparticles fabricated by nanosphere lithography. *Nano Lett.* **2005**, *5*, 1503-1507.

(59) Wiley, B.; Herricks, T.; Sun, Y.; Xia, Y. Polyol synthesis of silver nanoparticles: Use of chloride and oxygen to promote the formation of single-crystal, truncated cubes and tetrahedrons. *Nano Lett.* **2004**, *4*, 1733-1739.

(60) Yang, J.; Zhang, Q.; Lee, J. Y.; Too, H. Dissolution–recrystallization mechanism for the conversion of silver nanospheres to triangular nanoplates. *J. Colloid Interface Sci.* **2007**, *308*, 157-161.

(61) Elechiguerra, J. L.; Larios-Lopez, L.; Liu, C.; Garcia-Gutierrez, D.; Camacho-Bragado, A.; Yacaman, M. J. Corrosion at the nanoscale: The case of silver nanowires and nanoparticles. *Chem. Mater.* **2005**, *17*, 6042-6052.

(62) Hocking, M. B.; Bhandari, K.; Shell, B.; Smyth, T. A. Steric and pH effects on the rate of Dakin oxidation of acylphenols. *J. Org. Chem.* **1982**, *47*, 4208-4215.

(63) Liu, J.; Pennell, K. G.; Hurt, R. H. Kinetics and mechanisms of nanosilver oxysulfidation. *Environ. Sci. Technol.* **2011**, *45*, 7345-7353.

(64) Kapoor, S. Preparation, characterization, and surface modification of silver particles. *Langmuir* **1998**, *14*, 1021-1025.

(65) Henglein, A.; Linnert, T.; Mulvaney, P. Reduction of Ag^+ in aqueous polyanion solution: Some properties and reactions of long-lived oligomeric silver clusters and metallic silver particles. *Ber. Bunsen-Ges. Phys. Chem* **1990**, *94*, 1449-1457.

(66) Henglein, A.; Mulvaney, P.; Linnert, T. Chemistry of Ag_n, aggregates in aqueous solution: Non-metallic oligomeric clusters and metallic particles. *Faraday Discuss.* **1991**, *92*, 31-44.

(67) Mulvaney, P.; Linnert, T.; Henglein, A. Surface chemistry of colloidal silver in aqueous solution: Observations on chemisorption and reactivity. *J. Phys. Chem.* **1991**, *95*, 7843-7846.

(68) Shang, L.; Dong, S. Sensitive detection of cysteine based on fluorescent silver clusters. *Biosens. Bioelectron.* **2009**, *24*, 1569–1573.

(69) Strelow, F.; Henglein, A. Time resolved chemisorption of I⁻ and SH⁻ on colloidal silver particles (a stopped-flow study). *J. Phys. Chem.* **1995**, *99*, 11834-11838.

(70) Linnert, T.; Mulvaney, P.; Henglein, A. Surface chemistry of colloidal silver: Surface plasmon damping by chemisorbed I⁻, SH⁻, and $C_6H_5S^-$. *J. Phys. Chem.* **1993**, *97*, 679-682.

(71) Levard, C. M.; Reinsch, B. C.; Michel, F. M.; Oumahi, C.; Lowry, G. V.; Brown, G. E. Sulfidation processes of PVP-coated silver nanoparticles in aqueous solution: Impact on dissolution rate. *Environ. Sci. Technol.* **2011**, *45*, 5260-5266.

(72) Bell, R. A.; Kramer, J. R. Structural chemistry and geochemistry of silver-sulfur compounds: Critical review. *Environ. Toxicol. Chem.* **1999**, *18*, 9-22.

(73) Adams, N. W. H.; Kramer, J. R. Silver speciation in wastewater effluent, surface waters, and pore waters. *Environ. Toxicol. Chem.* **1999**, *18*, 2667-2673.

(74) Kramer, J. R.; Bell, R. A.; Smith, D. S. Determination of sulfide ligands and association with natural organic matter. *Appl. Geochem.* **2007**, *22*, 1606–1611.

(75) Rozan, T. F.; Lassman, M. E.; Ridge, D. P.; Luther, G. W. Evidence for iron, copper and zinc complexation as multinuclear sulphide clusters in oxic rivers. *Nature* **2000**, *406*, 879-882.

(76) Kim, B.; Park, C. S.; Murayama, M.; Hochella, M. F. Discovery and characterization of silver sulfide nanoparticles in final sewage sludge products. *Environ. Sci. Technol.* **2010**, *44*, 7509-7514.

(77) Jacobson, A. R.; Martinez, C. E.; Spagnuolo, M.; Mcbride, M. B.; Baveye, P. Reduction of silver solubility by humic acid and thiol ligands during acanthite (beta-Ag_2S) dissolution. *Environ. Pollut.* **2005**, *135*, 1-9.

(78) Krzewska, S.; Podsiadly, H. Complexes of Ag(I) with ligands containing sulphur donor atoms. *Polyhedron* **1986**, *5*, 937-944.

(79) Stebounova, L. V.; Guio, E.; Grassian, V. H. Silver nanoparticles in simulated biological media: A study of aggregation, sedimentation, and dissolution. *J. Nanopart. Res.* **2011**, *13*, 233–244.

(80) Rubasinghege, G.; Lentz, R. W.; Park, H.; Scherer, M. M.; Grassian, V. H. Nanorod dissolution quenched in the aggregated state. *Langmuir* **2010**, *26*, 1524-1527.

(81) Hotze, E. M.; Labille, J.; Alvarez, P.; Wiesner, M. R. Mechanisms of photochemistry and reactive oxygen production by fullerene suspensions in water. *Environ. Sci. Technol.* **2008**, *42*, 4175-4180.

(82) Hotze, E. M.; Bottero, J. Y.; Wiesner, M. R. Theoretical framework for nanoparticle reactivity as a function of aggregation state. *Langmuir* **2010**, *26*, 11170-11175.

(83) Bligh, M. W.; Waite, T. D. Formation, aggregation and reactivity of amorphous ferric oxyhydroxides on dissociation of Fe(III)-organic complexes in dilute aqueous suspensions. *Geochim. Cosmochim. Acta* **2010**, *74*, 5746-5762.

(84) Avouris, P. Manipulation of matter at the atomic and molecular-levels. *Accounts Chem. Res.* **1995**, *28*, 95-102.

(85) Piner, R. D.; Zhu, J.; Xu, F.; Hong, S. H.; Mirkin, C. A. "Dip-pen" nanolithography. *Science* **1999**, *283*, 661-663.

(86) Haynes, C. L.; Van Duyne, R. P. Nanosphere lithography: A versatile nanofabrication tool for studies of size-dependent nanoparticle optics. *J. Phys. Chem. B* **2001**, *105*, 5599-5611.

(87) Ito, T.; Okazaki, S. Pushing the limits of lithography. *Nature* **2000**, *406*, 1027-1031.

(88) Utke, I.; Hoffmann, P.; Melngailis, J. Gas-assisted focused electron beam and ion beam processing and fabrication. *J. Vac. Sci. Technol. B* **2008**, *26*, 1197-1276.

(89) Wallraff, G. M.; Hinsberg, W. D. Lithographic imaging techniques for the formation of nanoscopic features. *Chem. Rev.* **1999**, *99*, 1801-1821.

(90) Fischer, U. C.; Zingsheim, H. P. Sub-microscopic pattern replication with visible-light. *J. Vac. Sci. Technol.* **1981**, *19*, 881-885.

(91) Deckman, H. W.; Dunsmuir, J. H. Natural lithography. *Appl. Phys. Lett.* **1982**, *41*, 377-379.

(92) Ormonde, A. D.; Hicks, E. C. M.; Castillo, J.; Van Duyne, R. P. Nanosphere lithography: Fabrication of large-area Ag nanoparticle arrays by convective self-assembly and their characterization by scanning UV-visible extinction spectroscopy. *Langmuir* **2004**, *20*, 6927-6931.

(93) Hulteen, J. C.; Van Duyne, R. P. Nanosphere lithography - a materials general fabrication process for periodic particle array surfaces. *J. Vac. Sci. Technol. A-Vac. Surf. Films* **1995**, *13*, 1553-1558.

(94) Yang, S. M.; Jang, S. G.; Choi, D. G.; Kim, S.; Yu, H. K. Nanomachining by colloidal lithography. *Small* **2006**, *2*, 458-475.

(95) Prevo, B. G.; Kuncicky, D. M.; Velev, O. D. Engineered deposition of coatings from nano- and micro-particles: A brief review of convective assembly at high volume fraction. *Colloid Surf. A-Physicochem. Eng. Asp.* **2007**, *311*, 2-10.

(96) Deckman, H. W.; Dunsmuir, J. H. Applications of surface textures produced with natural lithography. *J. Vac. Sci. Technol. B* **1983**, *1*, 1109-1112.

(97) Deckman, H. W.; Dunsmuir, J. H.; Garoff, S.; Mchenry, J. A.; Peiffer, D. G. Macromolecular self-organized assemblies. *J. Vac. Sci. Technol. B* **1988**, *6*, 333-336.

(98) Hulteen, J. C.; Treichel, D. A.; Smith, M. T.; Duval, M. L.; Jensen, T. R.; Van Duyne, R. P. Nanosphere lithography: Size-tunable silver nanoparticle and surface cluster arrays. *J. Phys. Chem. B* **1999**, *103*, 3854-3863.

(99) Haynes, C. L.; Mcfarland, A. D.; Smith, M. T.; Hulteen, J. C.; Van Duyne, R. P. Angle-resolved nanosphere lithography: Manipulation of nanoparticle size, shape, and interparticle spacing. *J. Phys. Chem. B* **2002**, *106*, 1898-1902.

(100) Jensen, T. R.; Duval, M. L.; Kelly, K. L.; Lazarides, A. A.; Schatz, G. C.; Van Duyne, R. P. Nanosphere lithography: Effect of the external dielectric medium on the surface plasmon resonance spectrum of a periodic array of sliver nanoparticles. *J. Phys. Chem. B* **1999**, *103*, 9846-9853.

(101) Chen, X.; Wei, X.; Jiang, K. The fabrication of high-aspect-ratio, size-tunable nanopore arrays by modified nanosphere lithography. *Nanotechnology* **2009**, *20*.

(102) Malinsky, M. D.; Kelly, K. L.; Schatz, G. C.; Van Duyne, R. P. Nanosphere lithography: Effect of substrate on the localized surface plasmon resonance spectrum of silver nanoparticles. *J. Phys. Chem. B* **2001**, *105*, 2343-2350.

(103) Pacifico, J.; Jasieniak, J.; Gomez, D. E.; Mulvaney, P. Tunable 3D arrays of quantum dots: Synthesis and luminescence properties. *Small* **2006**, *2*, 199-203.

(104) Kempa, K.; Kimball, B.; Rybczynski, J.; Huang, Z. P.; Wu, P. F.; Steeves, D.; Sennett, M.; Giersig, M.; Rao, D.; Carnahan, D. L.; Wang, D. Z.; Lao, J. Y.; Li, W. Z.; Ren, Z. F. Photonic crystals based on periodic arrays of aligned carbon nanotubes. *Nano Lett.* **2003**, *3*, 13-18.

(105) Wang, X. D.; Summers, C. J.; Wang, Z. L. Large-scale hexagonal-patterned growth of aligned ZnO nanorods for nano-optoelectronics and nanosensor arrays. *Nano Lett.* **2004**, *4*, 423-426.

(106) Hasse, U.; Scholz, F. *In situ* AFM observation of the electrochemical reduction of a single silver sulphide crystal and the recrystallization of the resulting silver crystal. *Electrochem. Commun.* **2005**, *7*, 173-176.

(107) Lea, A. S.; Amonette, J. E.; Baer, D. R.; Liang, Y.; Colton, N. G. Microscopic effects of carbonate, manganese, and strontium ions on calcite dissolution. *Geochim. Cosmochim. Acta* **2001**, *65*, 369-379.

(108) Perry, T. D.; Duckworth, O. W.; Mcnamara, C. J.; Martin, S. T.; Mitchell, R. Effects of the biologically produced polymer alginic acid on macroscopic and microscopic calcite dissolution rates. *Environ. Sci. Technol.* **2004**, *38*, 3040-3046.

(109) Keller, D. Reconstruction of STM and AFM images distorted by finite-size tips. *Surf. Sci.* **1991**, *253*, 353-364.

(110) Chicon, R.; Ortuno, M.; Abellan, J. An algorithm for surface reconstruction in scanning tunneling microscopy. *Surf. Sci.* **1987**, *181*, 107-111.

(111) Lead, J. R.; Muirhead, D.; Gibson, C. T. Characterization of freshwater natural aquatic colloids by atomic force microscopy (AFM). *Environ. Sci. Technol.* **2005**, *39*, 6930-6936.

(112) Hutter, J. L.; Bechhoefer, J. Calibration of atomic-force microscope tips. *Rev. Sci. Instrum.* **1993**, *64*, 1868-1873.

(113) Odin, C.; Aime, J. P.; Elkaakour, Z.; Bouhacina, T. Tip finite-size effects on atomic-force microscopy in the contact mode - simple geometrical considerations for rapid estimation of apex radius and tip angle based on the study of polystyrene latex balls. *Surf. Sci.* **1994**, *317*, 321-340.

(114) Vesenka, J.; Manne, S.; Giberson, R.; Marsh, T.; Henderson, E. Colloidal gold particles as an incompressible atomic-force microscope imaging standard for assessing the compressibility of biomolecules. *Biophys. J.* **1993**, *65*, 992-997.

(115) Markiewicz, P.; Goh, M. C. Atomic-force microscopy probe tip visualization and improvement of images using a simple deconvolution procedure. *Langmuir* **1994**, *10*, 5-7.

2.8   TABLES AND FIGURES

Table 2-1: Modeled Concentrations of Silver in the Environment

| Compartment | European Union | | USA | Switzerland | | Unit |
	Gottschalk et al.[29,a]	Blaser et al.[30,b]	Gottschalk et al.[29,a]	Gottschalk et al.[29,a]	Mueller & Nowack[28,c]	
Surface water	0.764	140	0.116	0.717	0.03	ng/L
WWTP effluent	42.5	9000	21	38.7		ng/L

(a) Probability-based mode for nanosilver. (b) "Intermediate scenario" for *total* silver (not just nanosilver). (c) "Realistic scenario" for nanosilver.

3   Controlled Evaluation of the Effects of NaCl on Silver Nanoparticle Dissolution

3.1   INTRODUCTION

As a result of their biocidal properties, silver nanoparticles (AgNPs) have been incorporated into a wide range of consumer products, including textiles, plastics, cosmetics, household sprays, and paints with the total number of applications rapidly increasing.[1-3] There is significant potential for release of AgNPs from these products into the environment,[2,4,5] and this discharge into aquatic systems could have unintended detrimental ecological impacts.[1]

AgNP toxicity has been demonstrated for several species of vertebrates, invertebrates, and prokaryotic and eukaryotic microorganisms, as well as some mammalian cell lines and viruses.[1,6] Studies have shown that size,[7-9] shape,[10] surface coating,[11,12] and solution chemistry[13,14] all influence AgNP toxicity. The toxicity of the free silver ion, Ag^+, and its complexes has been well documented, but there is ongoing debate over whether the observed toxicity of AgNPs is due to the release of Ag^+ alone, or if the nanoparticles themselves exert a direct toxic effect.[14-16] Some researchers have suggested that AgNPs are similar to a drug delivery system in which the AgNPs transport and deliver biologically active Ag^+ to a biological target.[17] Under this paradigm, the biological activity of AgNPs is controlled by Ag^+ release rates, which, in turn, are controlled by size, shape, surface coating, and so forth.[17]

Even if Ag^+ is only partially responsible for the observed toxic effects of AgNPs, dissolution may still be an important environmental transformation that dictates the concentration and form of silver that aquatic organisms are exposed to. For this reason, several

studies have explored the dissolution kinetics of AgNPs under a variety of conditions;[17-21] however, particle aggregation was uncontrolled in each of these studies and the potential effects of aggregation on nanoparticle dissolution rates were given little to no attention. Recently, however, studies performed with magnetite[22] and galena[23] nanoparticles, goethite nanorods[24], and nC_{60} suspensions[25,26] have demonstrated that aggregation decreases nanomaterial reactivity by an order of magnitude or more. This decreased reactivity is explained in part by diminished particle surface area in contact with the solution phase and hindered mass transport to reactive sites within dense aggregate structures.[22,23]

The objective of this work was to use nanosphere lithography (NSL) to fabricate uniform arrays of AgNPs immobilized on glass substrates to enable the evaluation of AgNP dissolution under highly controlled conditions in the absence of aggregation. NSL is a versatile, inexpensive, and high-throughput lithographic technique that enables creation of periodic nano- and microparticle arrays.[27] NSL facilitates control over size, shape, and interparticle spacing for a number of different materials and substrates.[28-31] In this study, the dissolution rates of NSL-produced AgNPs were quantified by atomic force microscopy (AFM), which gave a detailed description of changes in particle size and shape as a function of time and NaCl concentration. This work demonstrates the utility of NSL for future studies examining nanomaterial fate in the environment.

3.2 MATERIALS AND METHODS

Dissolution experiments were conducted in phosphate buffers produced by dissolving 1 mM NaH_2PO_4 and 1 mM Na_2HPO_4 in air-saturated deionized (DI) water (18.2 MΩ cm, Barnstead). Aliquots of 5 M NaCl were added to the buffer to achieve variable NaCl concentrations (10-550 mM) and the solution pH was adjusted to 7.0 ± 0.1 using 0.1 N NaOH.

The highest NaCl concentration used is characteristic of seawater, while the lowest is approximately representative of cytoplasm.[17] All dissolution experiments were conducted at room temperature (25 °C) in the dark. Glass substrates ($60 \times 24 \times 0.15$ mm microscope cover glass, Fisher Scientific) were cleaned by immersion in a solution of 4% NH_4OH/16% H_2O_2 at 75 °C for 10 min, followed by an additional 10 min in 14% HCl/14% H_2O_2 at 75 °C. The substrates were rinsed thoroughly with DI water after each cleaning step and dried using filtered air after the final rinse. Glassware used for substrate production was cleaned similarly, and glassware used for acid digestion was cleaned by soaking overnight in 14% HNO_3 and was then rinsed with DI water.

3.2.1 Substrate Production

After cleaning, the glass substrates were thiolated by immersing them in 5% (3-mercaptopropyl)trimethoxysilane (Sigma-Aldrich) dissolved in spectrophotometric grade methanol (Alfa Aesar) overnight.[32] Thiol groups have a strong affinity for soft-metals such as silver, and preliminary experiments indicated that the AgNPs were highly mobile on the substrate if the glass was not thiolated prior to use. Following thiolation, glass substrates were rinsed with and stored in methanol until use.

Convective self-assembly (CSA), as described by Chen et al.,[33] was used to deposit a monolayer of 450-nm diameter carboxylated latex spheres (4% w/v, Invitrogen) onto the thiolated substrates. Briefly, the substrates were held horizontally on a motion stage (Thor Labs) approximately 10-200 μm below an angled plate. This CSA assembly was enclosed in an airtight container. Prior to surface application, centrifugation was used to concentrate the latex colloid suspension fivefold. A drop of this concentrated latex colloid suspension was placed between the substrate and the angled plate. The substrate was then moved at a constant velocity relative to the

plate, causing the colloidal suspension to be spread over the substrate. Solvent evaporation induces the latex spheres to crystallize into a hexagonally close-packed monolayer.

Following CSA, silver was vacuum deposited onto the substrates by electron beam evaporation (3-kW electron gun, Thermionics).[34] Prepared substrates were stored in sealed glass jars for periods up to several months until use. Immediately prior to use, substrates were cut into approximate 2×2 mm specimens and attached to 15-mm AFM specimen discs (Ted Pella) using wax. The latex spheres were then removed by sonication in ethanol for 1 min. Each specimen was rinsed in DI water for 1 min and dried with filtered air. ImageJ (NIH) was used to estimate the total area of each specimen based upon digital images.

The total amount of silver deposited was determined for five prepared specimens by placing each sample in 10 mL of 5% trace metal grade HNO_3 (Fisher Scientific)/3% H_2O_2 at 120 °C on a hot plate for 1 h followed by analysis of the supernatant via inductively coupled plasma-mass spectrometry (ICP-MS, Agilent 7500C). The solution volume was restored to 10 mL using DI water prior to ICP-MS analysis. A LEO (Zeiss) 1550 Schottky field-emission scanning electron microscope (SEM) equipped with an Oxford INCA Energy E2H X-ray energy dispersive spectrometer (EDS) system with silicon drift detector was used for SEM and EDS measurements. Samples were sputter coated with gold-palladium for 30 s prior to SEM imaging. SEM images were analyzed using ImageJ. X-ray photoelectron spectroscopy (XPS) was performed using a PHI Quantera XPS microprobe.

3.2.2 Nanoparticle Dissolution Experiments

After initial characterization by AFM, prepared specimens were submerged in 10 mL aqueous samples of variable NaCl concentrations in 15-mL polystyrene sample tubes (Fisher Scientific), sealed, and then placed in the dark. Each specimen was periodically removed from

solution for AFM characterization. Upon completion of the predetermined incubation period, the supernatant was acidified with 200 μL of 67-70% HNO_3 and analyzed by ICP-MS to determine the dissolved silver concentration.

A Nanoscope IIIa Multimode AFM (Digital Instruments) equipped with a J scanner and silicon probes (TESP, spring constant of 20-80 N/m, Bruker) was used to obtain all AFM data. All images were collected in tapping mode in air using a 256×256 pixel resolution at a scan rate of 0.5-1.0 Hz. Mean particle heights and radii were determined from 5×5 μm and 3×3 μm AFM images, where radius is defined as the radius of a circle of equivalent area, as described in Appendix A. The average number of particles measured to determine the mean particle height and radius at each time point was 142 with a minimum number of 42. High resolution AFM images (300×300 nm) were used for numerical volume integrations and the deconvolution procedure described below. The "Particle Analysis" extension of the NanoScope software was used with a threshold height of 10 nm for analysis of AFM data. Irregular particles resulting from defects in the latex colloid mask were excluded from analysis.

3.2.3 Data Analysis

A deconvolution algorithm developed by Markiewicz and Goh[35] was performed to estimate the correction factors used to account for distortions in lateral particle dimensions by the AFM probe. In essence, the algorithm places a facsimile of the known or assumed AFM probe shape, in this case a spherical tip with an 8-nm radius, at each data point and compares the geometry of the probe with the surrounding data points. Data points that conflict with the probe geometry have their height decreased to the highest point at which there is no conflict. Based on results from this technique, a radius correction factor of 6 nm was estimated for the initial time point, and a correction factor of 7 nm was used for subsequent time points in all instances except

for the case where no NaCl was added to the phosphate buffer; under the latter conditions no significant change in the particle shape was observed during the timeframe of the experiment.

To convert AFM mean height and corrected mean radius measurements to average particle volumes, a mathematical description of the corroded particle shape was formulated. High resolution AFM images of individual AgNPs were deconvoluted according to the method described in the preceding paragraph and then a numerical integration was performed to estimate the volume of individual particles. Several geometric shapes were assumed, using particle height and corrected radius as shape descriptors, and their volumes were compared with the integrated volumes. Additional details on this procedure are included in Appendix A. The shape whose calculated volume most closely predicted the integrated volumes is described by Equation 3-1.

$$y = h\left[1 - \left(\frac{x}{r}\right)^6\right]$$
(3-1)

where h is the measured particle height (nm), r is the corrected particle radius (nm), and x is the horizontal distance from the particle center (nm). Equation 3-1 is defined for $0 \leq x \leq r$, and the 3-dimensional shape is obtained by revolving this function 2π radians about the y-axis. Equation 3-2 was determined by integration and gives the volume, V_p (nm^3), of the particle described by Equation 3-1.

$$V_p = \frac{3\pi}{4} h r^2$$
(3-2)

Changes in average particle volume between time points were converted into a predicted aqueous silver concentration, C (µg/L ~ ppb), using Equation 3-3.

$$C = \frac{\rho(\Delta V_p)NA}{V_s}$$
(3-3)

41

where ρ is the density of bulk silver (1.05×10^{-14} µg/nm^3), N is the number of particles per unit substrate area assuming that the substrates are completely homogeneous (10 particles/µm^2), A is the total area of the specimen (µm^2), and V_s is the solution volume (0.01 L). We emphasize that given that the substrates produced by CSA are not homogeneous, the predicted concentration of silver in suspension obtained using Equation 3-3 is a highly conservative estimate, as discussed fully in the Results and Discussion.

3.3   RESULTS AND DISCUSSION

3.3.1   Substrate Characterization

A representative SEM micrograph of a finished AgNP array is shown in Figure 3-1a. Defect-free domains spanned several µm^2 and both point and line defects are evident. Initial characterization by AFM revealed that the NSL-produced AgNPs had a truncated tetrahedral shape as expected based upon past reports.[27-30] The nanoparticle heights were normally distributed with a mean value of 53.4 nm and a standard deviation of 2.5 nm (Figure 3-1b). AFM measurements, corrected as detailed in the Materials and Methods, gave a mean particle radius of 56.0 nm, which qualitatively agrees with the mean radius of 55.0 nm determined by SEM. The particle radius distribution was positively skewed with a standard deviation of 4 nm (Figure 3-1c). Numerical integration of high-resolution AFM data yielded an average volume of 3.1×10^5 nm^3/particle, which leads to a predicted silver mass for a hypothetical completely homogeneous substrate of 33 mg/m^2. The total silver determined by ICP-MS was 106 ± 24 mg/m^2. As expected, the value measured by ICP-MS was higher than the value predicted for a homogeneous substrate since the defects shown in Figure 3-1a contribute more mass per unit area than the individual particles. Numerous attempts to produce defect free substrates were unsuccessful – presumably due to surface heterogeneities in the glass substrates.

3.3.2   Change in Silver Nanoparticle Shape

During the first day of exposure to solutions of ≥10 mM NaCl, the in-plane AgNP shape changed from triangular to circular, the sidewalls steepened, and the height increased by 6-12 nm (Figure 3-2). Similar changes were observed for 1 mM NaCl, but the particles maintained their triangular in-plane shape. Changes in AgNP shape induced by chloride are often ascribed to a dissolution-recrystallization mechanism;[36,37] however, previous studies invariably involve a reductant and a surfactant, so these previous results are not directly comparable to those presented here and several other explanations had to be considered. SEM images (Appendix B, Figure B-1) indicated that highly irregular aggregates formed in NaCl solutions to some extent in spite of the thiolation procedure; however, these aggregates were entirely excluded from the AFM analysis, so an aggregation-based mechanism was immediately rejected. The possibility that the formation of a precipitate led to the observed height increase was evaluated theoretically and experimentally. Equilibrium calculations performed using Visual MINTEQ 2.53 predicted that no precipitate ($AgCl$, Ag_3PO_4, or Ag_2CO_3) would form under the experimental conditions of this study. In samples where a height change was observed, XPS did not detect Cl 2p and Cl 2s peaks near 200 and 270 eV, respectively, and EDS did not detect Cl K_α and K_β peaks near 2.6 and 2.8 keV, indicating that an AgCl precipitate was not present. Based on this evidence, we can safely conclude that the measured change in height was not due to precipitation.

Upon careful examination of the literature, a hypothesis was qualitatively formulated that involves a redox potential gradient within each individual NSL-produced AgNP. Zhang et al. reported that NSL-produced AgNPs dissolve at the bottom edges first, then at the triangular corners, and finally at the out-of-plane height during electrochemical processing, thus suggesting that a redox potential gradient exists within an individual nanoparticle.[38] They attributed this

result to the sharp radius of curvature along the particles' bottom edges and corners. Surface free energy contributes substantially to the total free energy for features that exhibit sharp radii of curvature, and this excess surface energy can lead to a more negative redox potential at these sites.[39,40] Ag^+ is known to exist on AgNP surfaces in air-saturated water,[12,18] and we hypothesize that oxidation of Ag^0 to Ag^+ occurred at the bottom edges and corners of the AgNPs (the anode), while reduction of Ag^+ to Ag^0 occurred at their tops (the cathode). This process formed a Ag^+ concentration gradient that favored a net flow of silver from the bottom of a nanoparticle to the top until the internal redox potential gradient was eliminated. This hypothesis is consistent with the observed initial increase in AgNP height with a concomitant steepening of the sidewalls and dissolution at the corners.

This process was only apparent in NaCl solutions and did not occur in the phosphate buffer alone, thus suggesting a catalytic or reactive role for NaCl. Chloride has been observed in our study and others to catalyze oxidation of AgNPs,[36,37,41,42] which may be explained by the "pre-oxidation" or "pre-complexation" mechanism proposed by Henglein and coworkers.[43,44] They postulated that nucleophiles coordinated to an AgNP surface would force excess negative charge into the AgNP interior; thus, chloride apparently helps overcome the energy barrier to oxidation by promoting electron transfer through the AgNP interior. Additional experimentation, which was outside the scope of the present effort focused on nanoparticle dissolution, is required to fully evaluate the hypothesis that internal redox potential gradients were responsible for the initial change in height. To date we are unaware of any previous studies that have illustrated this important short-term change in particle morphology.

3.3.3 Dissolution Rates

After the first day, both the mean particle height and radius decreased linearly with time (Figure 3-3). The dissolution rates (i.e., the slopes of the linear regressions) were significant ($p < 0.05$) for all the data shown except for the case where no NaCl was added. As shown in Figure 3-3c, there is a strong linear correlation between the AgNP dissolution rate and the concentration of NaCl ($R^2 = 0.999$) and the measured dissolution rates were the same, within error, for both particle height and radius measurements. Empirical formulas for predicting AgNP dissolution rates as a function of NaCl concentration in units of nm/d and $mg/m^2/d$ are included in Appendix C, but the applicability of these formulas is limited to the experimental conditions of this study (e.g., pH 7, 25 °C, phosphate buffer). If the regression lines are extrapolated to the low NaCl concentrations expected in freshwater (0.1-1 mM), then the effect of NaCl is minimal (i.e., the dissolution rate is predicted to increase by only 0.03 nm/d over the range of 0-10 mM NaCl). On the other hand, the dissolution rate is predicted to increase nearly 6× at NaCl concentrations typical of seawater (i.e., 2.2 nm/d for 550 mM NaCl compared with ~0.4 nm/d for ≤10 mM NaCl).

Because hydrogen ions and oxygen are consumed during the dissolution reaction, changes in pH and the dissolved oxygen concentration can influence the observed dissolution rates.[18,19] Since the solutions used in this study were air saturated (0.20-0.26 mM O_2), the dissolved oxygen levels were approximately three orders of magnitude larger than the highest silver concentration (~0.0003 mM Ag^+); therefore, the dissolved oxygen concentration can be considered constant. Furthermore, the pH of the solutions was well buffered, with the pH in three 550 mM NaCl solutions stable at 7.0 ± 0.1 at the end of a 2-week dissolution period.

By using the regression equations from Figure 3-3 in conjunction with Equations 3-2 and 3-3, the dissolved silver concentration was calculated as a function of time and compared with ICP-MS measurements. Standards and controls indicated that the NaCl matrix caused the ICP-MS analysis to underestimate the actual silver concentration by as much as 40%. Despite the low recoveries, the predicted values were of the same order of magnitude as the actual silver concentrations assuming that the raw measured value and the measured value after adjustment for a 40% error are the lower and upper bounds, respectively (Figure 3-4). The predicted silver concentration was clearly lower than the real values for NaCl concentrations >300 mM because the calculation underestimates the total silver available for dissolution, as noted previously. Thus, the ICP-MS analysis, while not truly quantitative, agrees with the AFM results.

The predicted concentrations obtained from the AFM results were fit with a pseudo-first-order kinetic model to approximate mass-based first-order rate constants for comparison with values found in the literature (see Appendix D for details). The rate constants increased linearly between 0.01 and 0.10 d^{-1} over the 10-550 mM NaCl range. These first-order rate constants are lower than rate constants reported in previous studies on AgNP dissolution, which is contrary to expectations because the catalytic effect of NaCl is absent from the previous studies;[18-20] however, mass-based rate constants are not always comparable for surface-mediated reactions. For example, one study showed that three mass-based silver dissolution rate constants that varied by five orders of magnitude were all consistent with a surface area normalized rate constant of 2 nm/d.[17] Thus, reporting mass-based rate constants for AgNP dissolution may have little practical value. Interestingly, the 2 nm/d dissolution rate reported was for a pH 4 acetate buffer,[17] which is the same dissolution rate observed in this study for pH 7 and 550 mM NaCl. Given the

accelerated dissolution of AgNPs at low pH,[18] this surface area normalized comparison is consistent with the observation that NaCl enhances AgNP dissolution rates.

Although our results and others indicate that chloride will catalyze AgNP dissolution, Liu and Hurt observed a slight inhibition of AgNP dissolution in seawater.[18] AgCl precipitation could have diminished Ag^+ release, but the authors' equilibrium calculations predicted that nearly 100% of dissolved silver would be present as soluble chloride complexes in their system. Their seawater matrix may have hindered their Ag^+ measurements, similar to what occurred with the ICP-MS analysis in this study, but the authors did not give any indication that such interference occurred. Another possibility is that some component of the seawater prevented NaCl-enhanced corrosion of the AgNPs. Importantly, Liu and Hurt observed that AgNPs aggregated in the seawater, but they concluded that neither ionic strength nor aggregation had a strong influence on the dissolution kinetics.[18] In this study, we have clearly demonstrated that NaCl enhances AgNP dissolution, and it is thus reasonable to conclude that AgNP aggregation in the samples studied by Liu and Hurt may have had a quenching effect similar in magnitude to the catalyzing influence of the high NaCl concentration in seawater. Past studies with iron oxides and galena have indicated the importance of aggregation state on nanomaterial dissolution rates.[23,24]

To further explore the hypothesis that aggregation impedes AgNP dissolution we offer alternate interpretations of previous results. Kittler et al. observed that poly(vinylpyrrolidone) (PVP)-coated AgNPs dissolved more rapidly than citrate-coated AgNPs, but no explanation for this result was given.[20] PVP stabilizes AgNPs against aggregation more effectively than citrate,[42] so the increased dissolution rate of PVP-coated AgNPs could be due to decreased aggregation. It has also been reported that AgNPs achieve a pseudo-equilibrium that is dependent on the initial

AgNP concentration and size, a hypothesis explained by citing the size-dependent thermodynamic properties of AgNPs,[19,20] and that mass-based AgNP dissolution rate constants decreased as the concentration of AgNPs increased.[18,19] Both these phenomena could be caused by the depletion of molecular oxygen and hydrogen ions;[18,20] however, this possibility does not appear to hold in at least one case where these trends are apparent.[19] Another interpretation is that aggregation and dissolution act as competing processes, both of which depend on initial nanoparticle concentration and size. At higher AgNP concentrations, more inter-particle collisions lead to more rapid aggregation causing dissolution rate constants to decline. The pseudo-equilibrium could be a function of how much Ag^+ was released before aggregation almost completely quenched the dissolution reaction.

3.3.4 Environmental Implications

Because NaCl is ubiquitous in natural waters, it will potentially have a strong influence on the environmental dissolution kinetics of AgNPs, particularly in saline waters and biological media. Laboratory investigations are often confounded by precipitation of AgCl at the high AgNP concentrations used in many studies.[41,45] Recognizing the possibility of AgCl precipitation, one research group excluded Cl$^-$ from an otherwise realistic aqueous medium.[19] Thus, many laboratory studies may underestimate realistic AgNP dissolution rates. The experimental technique employed herein overcomes this dilemma by eliminating the potentially confounding use of high AgNP concentrations.

As discussed, aggregation may quench AgNP dissolution. High ionic strength can lead to rapid AgNP aggregation, but polymer coatings and adsorbed humic substances can provide added stability by an electrosteric mechanism.[42] AgNPs that are electrosterically stabilized may experience only slight aggregation in high ionic strength waters, so dissolution may govern

AgNP fate in this scenario. Future efforts will focus on using NSL to investigate the effects of surface coating, size, and shape on AgNP dissolution under various environmental conditions in the absence of aggregation. Information obtained from these experiments is essential to understanding the interplay between dissolution and aggregation processes and the ultimate fate of AgNPs in the environment.

3.4 REFERENCES

(1) Fabrega, J.; Luoma, S. N.; Tyler, C. R.; Galloway, T. S.; Lead, J. R. Silver nanoparticles: Behaviour and effects in the aquatic environment. *Environ. Int.* **2011**, *37*, 517-531.

(2) Benn, T. M.; Westerhoff, P. Nanoparticle silver released into water from commercially available sock fabrics. *Environ. Sci. Technol.* **2008**, *42*, 4133–4139.

(3) Mueller, N. C.; Nowack, B. Exposure modeling of engineered nanoparticles in the environment. *Environ. Sci. Technol.* **2008**, *42*, 4447-4453.

(4) Geranio, L.; Heuberger, M.; Nowack, B. The behavior of silver nanotextiles during washing. *Environ. Sci. Technol.* **2009**, *43*, 8113–8118.

(5) Gottschalk, F.; Nowack, B. The release of engineered nanomaterials to the environment. *J. Environ. Monit.* **2011**, *13*, 1145-1155.

(6) Marambio-Jones, C.; Hoek, E. M. V. A review of the antibacterial effects of silver nanomaterials and potential implications for human health and the environment. *J. Nanopart. Res.* **2010**, *12*, 1531–1551.

(7) Morones, J. R.; Elechiguerra, J. L.; Camacho, A.; Holt, K.; Kouri, J. B.; Ramirez, J. T.; Yacaman, M. J. The bactericidal effect of silver nanoparticles. *Nanotechnology* **2005**, *16*, 2346-2353.

(8) Choi, O.; Hu, Z. Q. Size dependent and reactive oxygen species related nanosilver toxicity to nitrifying bacteria. *Environ. Sci. Technol.* **2008**, *42*, 4583-4588.

(9) Elechiguerra, J. L.; Burt, J. L.; Morones, J. R.; Camacho-Bragado, A.; Gao, X.; Lara, H. H.; Yacaman, M. J. Interaction of silver nanoparticles with HIV-1. *J. Nanobiotechnology* **2005**, *3*, 6-15.

(10) Pal, S.; Tak, Y. K.; Song, J. M. Does the antibacterial activity of silver nanoparticles depend on the shape of the nanoparticle? A study of the gram-negative bacterium *Escherichia Coli*. *Appl. Environ. Microbiol.* **2007**, *73*, 1712-1720.

(11) Kvitek, L.; Panacek, A.; Soukupova, J.; Kolar, M.; Vecerova, R.; Prucek, R.; Holecova, M.; Zboril, R. Effect of surfactants and polymers on stability and antibacterial activity of silver nanoparticles (NPs). *J. Phys. Chem. C* **2008**, *112*, 5825-5834.

(12) Lok, C.; Ho, C.; Chen, R.; He, Q.; Yu, W.; Sun, H.; Tam, P.; Chiu, J.; Che, C. Silver nanoparticles: Partial oxidation and antibacterial activities. *J. Biol. Inorg. Chem.* **2007**, *12*, 527-534.

(13) Gao, J.; Youn, S.; Hovsepyan, A.; Llaneza, V. L.; Wang, Y.; Bitton, G.; Bonzongo, J. C. J. Dispersion and toxicity of selected manufactured nanomaterials in natural river water samples: Effects of water chemical composition. *Environ. Sci. Technol.* **2009**, *43*, 3322-3328.

(14) Fabrega, J.; Fawcett, S. R.; Renshaw, J. C.; Lead, J. R. Silver nanoparticle impact on bacterial growth: Effect of pH, concentration, and organic matter. *Environ. Sci. Technol.* **2009**, *43*, 7285-7290.

(15) Sotiriou, G. A.; Pratsinis, S. E. Antibacterial activity of nanosilver ions and particles. *Environ. Sci. Technol.* **2010**, *44*, 5649-5654.

(16) Navarro, E.; Piccapietra, F.; Wagner, B.; Marconi, F.; Kaegi, R.; Odzak, N.; Sigg, L.; Behra, R. Toxicity of silver nanoparticles to *Chlamydomonas Reinhardtii*. *Environ. Sci. Technol.* **2008**, *42*, 8959-8964.

(17) Liu, J.; Sonshine, D. A.; Shervani, S.; Hurt, R. H. Controlled release of biologically active silver from nanosilver surfaces. *ACS Nano* **2010**, *4*, 6903–6913.

(18) Liu, J.; Hurt, R. H. Ion release kinetics and particle persistence in aqueous nano-silver colloids. *Environ. Sci. Technol.* **2010**, *44*, 2169–2175.

(19) Zhang, W.; Yao, Y.; Sullivan, N.; Chen, Y. S. Modeling the primary size effects of citrate-coated silver nanoparticles on their ion release kinetics. *Environ. Sci. Technol.* **2011**, *45*, 4422-4428.

(20) Kittler, S.; Greulich, C.; Diendorf, J.; Koller, M.; Epple, M. Toxicity of silver nanoparticles increases during storage because of slow dissolution under release of silver ions. *Chem. Mater.* **2010**, *22*, 4548-4554.

(21) Levard, C. M.; Reinsch, B. C.; Michel, F. M.; Oumahi, C.; Lowry, G. V.; Brown, G. E. Sulfidation processes of PVP-coated silver nanoparticles in aqueous solution: Impact on dissolution rate. *Environ. Sci. Technol.* **2011**, *45*, 5260-5266.

(22) Vikesland, P. J.; Heathcock, A. M.; Rebodos, R. L.; Makus, K. E. Particle size and aggregation effects on magnetite reactivity toward carbon tetrachloride. *Environ. Sci. Technol.* **2007**, *41*, 5277-5283.

(23) Liu, J.; Aruguete, D. M.; Murayama, M.; Hochella, M. F. Influence of size and aggregation on the reactivity of an environmentally and industrially relevant manomaterial (PbS). *Environ. Sci. Technol.* **2009**, *43*, 8178-8183.

(24) Rubasinghege, G.; Lentz, R. W.; Park, H.; Scherer, M. M.; Grassian, V. H. Nanorod dissolution quenched in the aggregated state. *Langmuir* **2010**, *26*, 1524-1527.

(25) Hotze, E. M.; Labille, J.; Alvarez, P.; Wiesner, M. R. Mechanisms of photochemistry and reactive oxygen production by fullerene suspensions in water. *Environ. Sci. Technol.* **2008**, *42*, 4175-4180.

(26) Hotze, E. M.; Bottero, J. Y.; Wiesner, M. R. Theoretical framework for nanoparticle reactivity as a function of aggregation state. *Langmuir* **2010**, *26*, 11170-11175.

(27) Haynes, C. L.; Van Duyne, R. P. Nanosphere lithography: A versatile nanofabrication tool for studies of size-dependent nanoparticle optics. *J. Phys. Chem. B* **2001**, *105*, 5599-5611.

(28) Haynes, C. L.; Mcfarland, A. D.; Smith, M. T.; Hulteen, J. C.; Van Duyne, R. P. Angle-resolved nanosphere lithography: Manipulation of nanoparticle size, shape, and interparticle spacing. *J. Phys. Chem. B* **2002**, *106*, 1898-1902.

(29) Hulteen, J. C.; Treichel, D. A.; Smith, M. T.; Duval, M. L.; Jensen, T. R.; Van Duyne, R. P. Nanosphere lithography: Size-tunable silver nanoparticle and surface cluster arrays. *J. Phys. Chem. B* **1999**, *103*, 3854-3863.

(30) Hulteen, J. C.; Vanduyne, R. P. Nanosphere lithography - a materials general fabrication process for periodic particle array surfaces. *J. Vac. Sci. Technol. A-Vac. Surf. Films* **1995**, *13*, 1553-1558.

(31) Jensen, T. R.; Duval, M. L.; Kelly, K. L.; Lazarides, A. A.; Schatz, G. C.; Van Duyne, R. P. Nanosphere lithography: Effect of the external dielectric medium on the surface plasmon resonance spectrum of a periodic array of sliver nanoparticles. *J. Phys. Chem. B* **1999**, *103*, 9846-9853.

(32) Grabar, K. C.; Freeman, R. G.; Hommer, M. B.; Natan, M. J. Preparation and characterization of au colloid monolayers. *Anal. Chem.* **1995**, *67*, 735-743.

(33) Chen, K.; Stoianov, S. V.; Bangerter, J.; Robinson, H. D. Restricted meniscus convective self-assembly. *J. Colloid Interface Sci.* **2010**, *344*, 315-320.

(34) Chen, K.; Durak, C.; Heflin, J. R.; Robinson, H. D. Plasmon-enhanced second-harmonic generation from ionic self-assembled multilayer films. *Nano Lett.* **2007**, *7*, 254-258.

(35) Markiewicz, P.; Goh, M. C. Atomic-force microscopy probe tip visualization and improvement of images using a simple deconvolution procedure. *Langmuir* **1994**, *10*, 5-7.

(36) Wiley, B.; Herricks, T.; Sun, Y.; Xia, Y. Polyol synthesis of silver nanoparticles: Use of chloride and oxygen to promote the formation of single-crystal, truncated cubes and tetrahedrons. *Nano Lett.* **2004**, *4*, 1733-1739.

(37) Yang, J.; Zhang, Q.; Lee, J. Y.; Too, H. Dissolution–recrystallization mechanism for the conversion of silver nanospheres to triangular nanoplates. *J. Colloid Interface Sci.* **2007**, *308*, 157-161.

(38) Zhang, X.; Hicks, E. M.; Zhao, J.; Schatz, G. C.; Van Duyne, R. P. Electrochemical tuning of silver nanoparticles fabricated by nanosphere lithography. *Nano Lett.* **2005**, *5*, 1503-1507.

(39) Plieth, W. J. Electrochemical properties of small clusters of metal atoms and their role in surface enhanced raman scattering. *J. Phys. Chem.* **1982**, *86*, 3166-3170.

(40) Redmond, P. L.; Hallock, A. J.; Brus, L. E. Electrochemical Ostwald ripening of colloidal Ag particles on conductive substrates. *Nano Lett.* **2005**, *5*, 131-135.

(41) Li, X.; Lenhart, J. J.; Walker, H. W. Dissolution-accompanied aggregation kinetics of silver nanoparticles. *Langmuir* **2010**, *26*, 16690-16698.

(42) Huynh, K. A.; Chen, K. L. Aggregation kinetics of citrate and polyvinylpyrrolidone coated silver nanoparticles in monovalent and divalent electrolyte solutions. *Environ. Sci. Technol.* **2011**, *45*, 5564-5571.

(43) Henglein, A.; Linnert, T.; Mulvaney, P. Reduction of Ag^+ in aqueous polyanion solution: Some properties and reactions of long-lived oligomeric silver clusters and metallic silver particles. *Ber. Bunsen-Ges. Phys. Chem* **1990**, *94*, 1449-1457.

(44) Henglein, A.; Mulvaney, P.; Linnert, T. Chemistry of Ag_n, aggregates in aqueous solution: Non-metallic oligomeric clusters and metallic particles. *Faraday Discuss.* **1991**, *92*, 31-44.

(45) Scheckel, K. G.; Luxton, T. P.; El Badawy, A. M.; Impellitteri, C. A.; Tolaymat, T. M. Synchrotron speciation of silver and zinc oxide nanoparticles aged in a kaolin suspension. *Environ. Sci. Technol.* **2010**, *44*, 1307-1312.
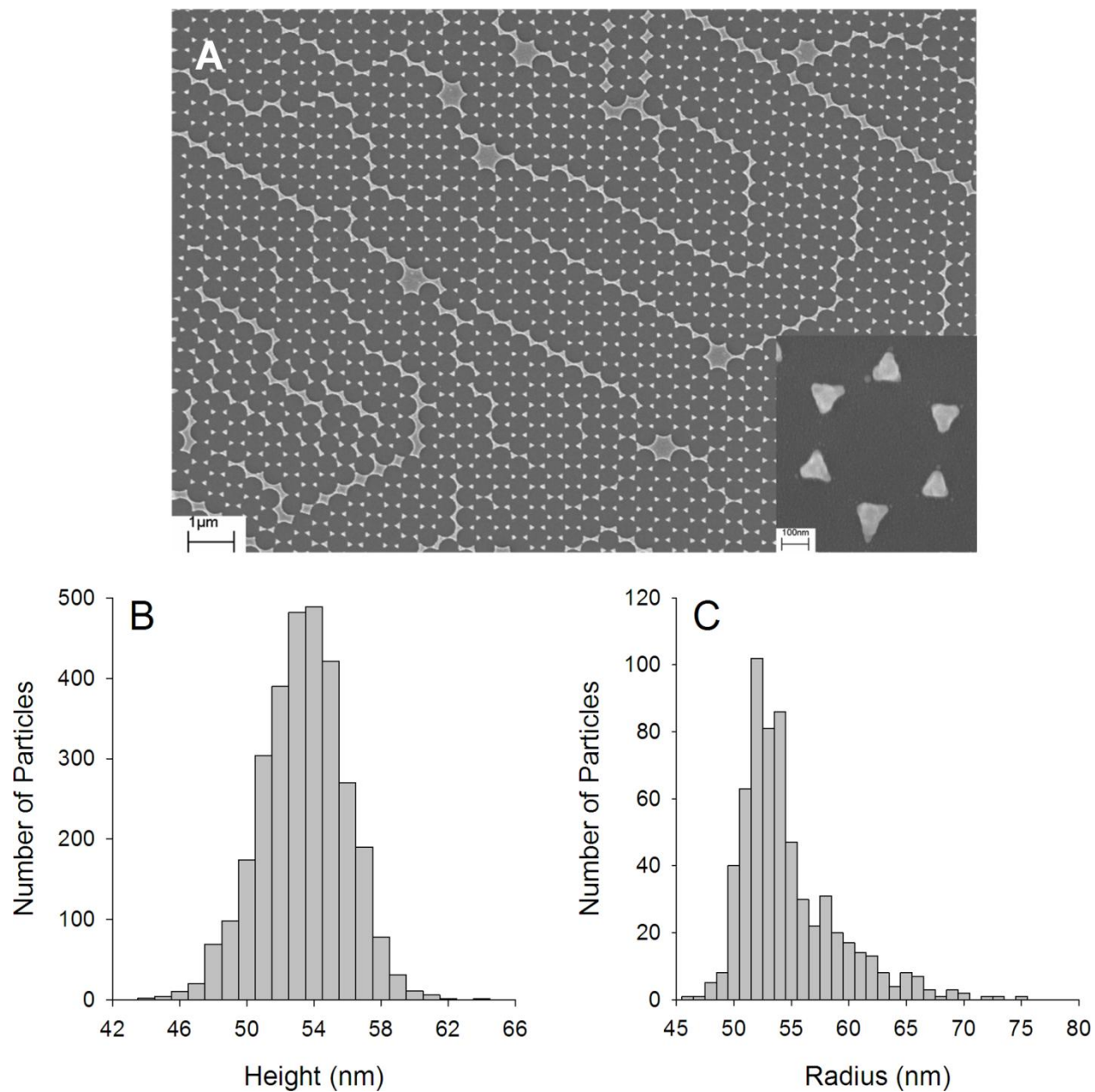
3.5   TABLES AND FIGURES

Figure 3-1. A) SEM micrograph of a typical NSL-produced AgNP array. B) Height (N = 3051) and C) radius (N = 620) distributions measured by AFM and SEM, respectively, for the AgNP arrays used in this study.
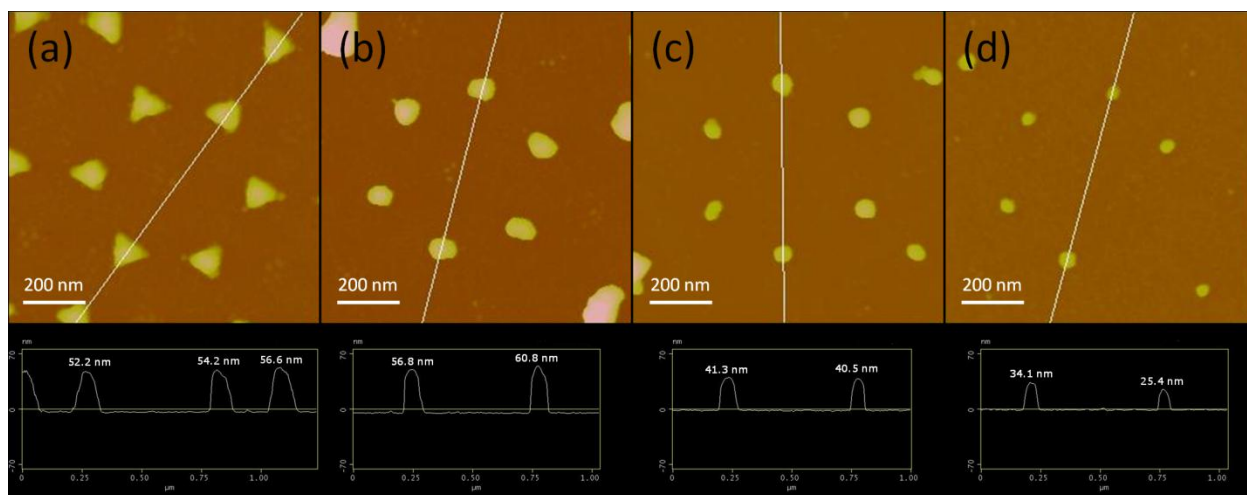
Figure 3-2. Deconvoluted AFM micrographs and height profiles for NSL-produced AgNP arrays (a) prior to initiation of a dissolution experiment and after (b) 1 d, (c) 7 d, and (d) 15 d of immersion in a 550 mM NaCl phosphate buffer at pH 7 and 25 °C. The four images were acquired at four different locations.
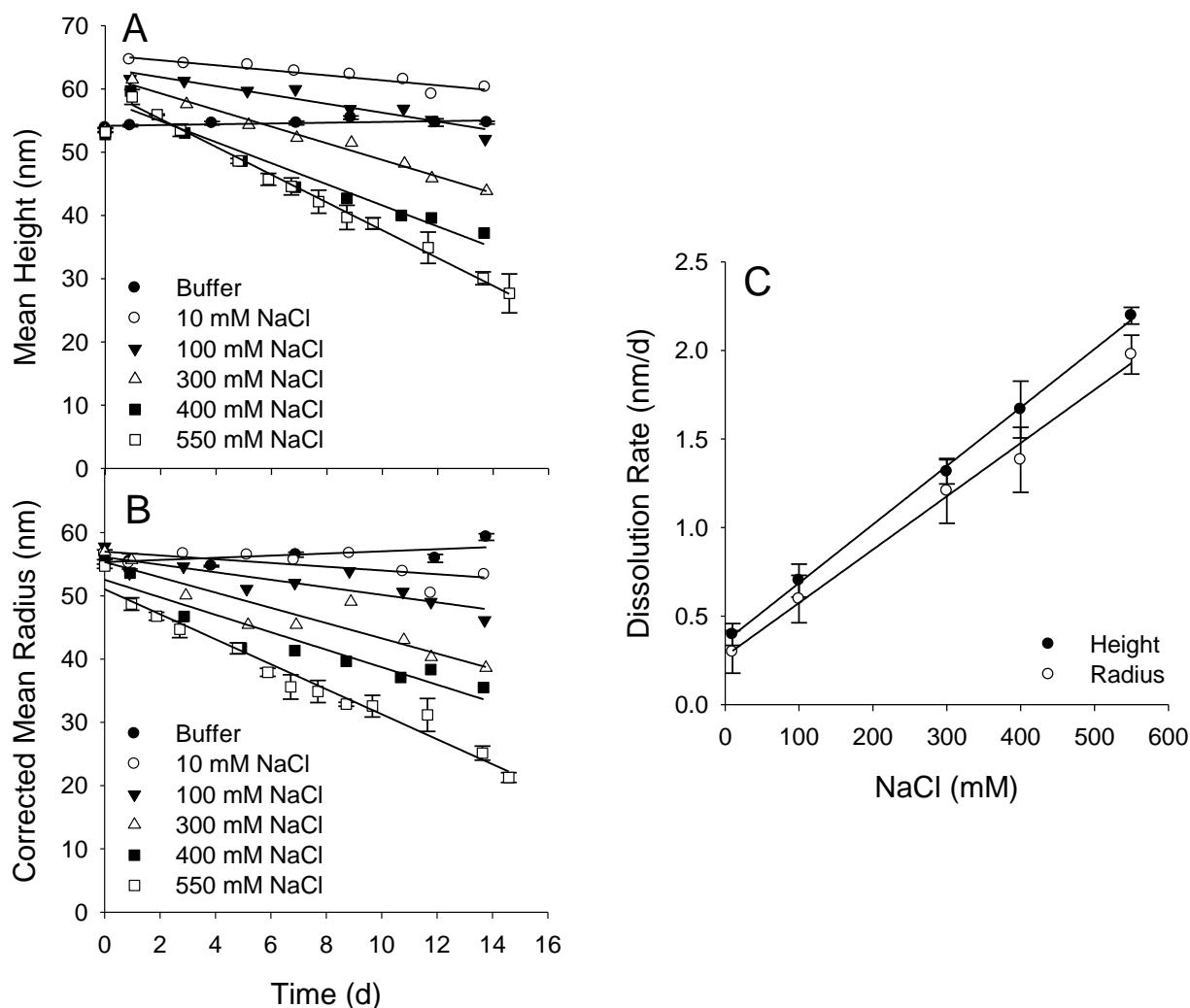
Figure 3-3. Results of AFM measurements for AgNP dissolution experiments. Variation of mean AgNP A) height and B) radius with time at different NaCl concentrations. Error bars, where shown, represent the standard deviation between mean heights or radii determined by AFM for experiments performed in triplicate. Three mean radius measurements were excluded because assumptions about the tip shape were obviously violated. C) Slopes of the regression lines for AgNP height and radius as a function of NaCl concentration. Standard errors are indicated by the error bars.
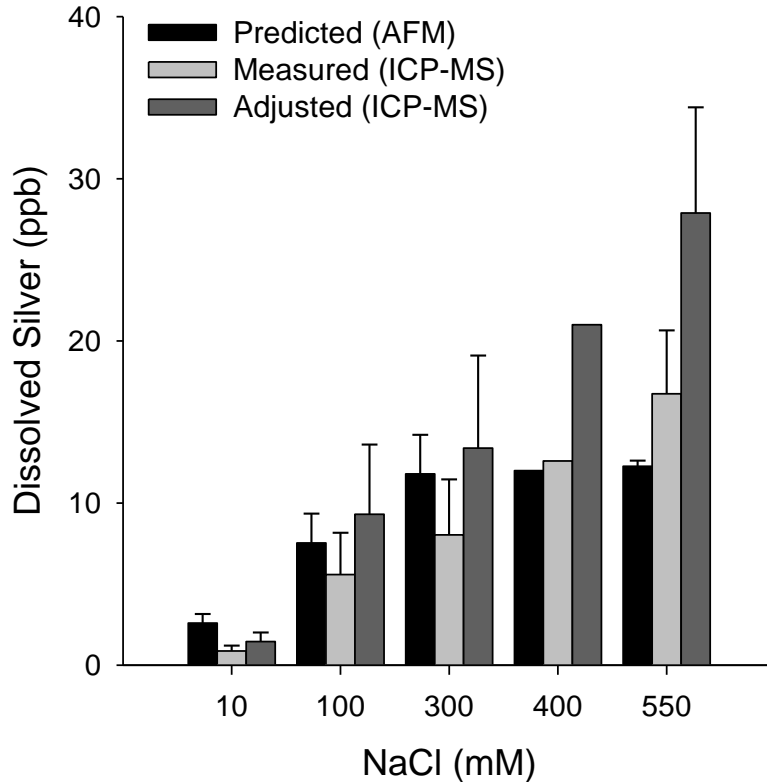
Figure 3-4. Predicted and measured dissolved silver in solutions of varying NaCl concentrations after approximately 2 weeks of NSL-produced AgNP dissolution. The predicted values are based on linear regression of AFM data (Figure 3-3) in conjunction with Equations 3-2 and 3-3. ICP-MS was used for the measured values, but quality controls indicated that the measured values underestimated the true values by up to 40%. The adjusted ICP-MS data corrects for a 40% underestimate (i.e., measured value/0.6) and represents an upper bound of the true Ag^+ concentration. Error bars for the calculated concentrations represent predicted standard deviations based on variations in the total specimen area and the incubation time, error bars for the measured concentrations represent the standard deviation of experiments performed in triplicate, and error bars for the adjusted concentrations are the standard deviation of the adjusted triplicate samples.

4   Engineering Significance

It was demonstrated herein that nanosphere lithography (NSL) and atomic force microscopy (AFM) could be used together to study silver nanoparticle (AgNP) dissolution without the confounding influence of aggregation. Not only was this experimental technique successful at measuring dissolution rates, but it also gave a detailed description of changes in AgNP morphology during the dissolution process. Uncoupling nanoparticle aggregation from dissolution opens the way to isolating the effects of size, shape, surface coating, and solution chemistry on AgNP dissolution. Once the influence of each of these factors is well characterized individually, then greater insight into the interplay between AgNP aggregation and dissolution can be developed, which will lead to a better understanding of how AgNPs will behave in the environment. This understanding can assist in managing and mitigating the potential risks of AgNP release into natural aquatic systems. The experimental technique employed in this work also has the potential to be extended to other nanomaterials that are of concern to the environment.

In addition to demonstrating a unique method for investigating AgNP dissolution, this study also showed how NaCl can accelerate AgNP dissolution rates. The results suggest that the high levels of NaCl present in biological media and saline waters have the potential to significantly enhance the release of Ag^+ from AgNPs. Since NaCl is ubiquitous in the environment, future research on AgNP dissolution kinetics should include NaCl if the results are to be considered environmentally relevant; otherwise, the measured dissolution rates may underestimate what can really be expected in the environment. Since NaCl can complicate AgNP studies by AgCl precipitation, it is also important that future studies be carried out at AgNP

concentrations that approach the levels expected in the environment where AgCl precipitation is less likely to occur.

Appendix A: Mathematical Description of Silver Nanoparticle Shape

A mathematical description of the corroded AgNP shape was necessary for prediction of the aqueous silver ion concentrations. Shape descriptors for the particle shapes were the measured particle height, h (nm), and radius, r (nm), where r is defined by Equation A-1.

$$r = \sqrt{\frac{A_p}{\pi}}$$
(A-1)

where A_p (nm^2) is the area of the 2-dimensional projection of a particle's in-plane shape measured by AFM or SEM. The mathematical form for describing the corroded AgNPs is given in Equation A-2.

$$y = h\left[1 - \left(\frac{x}{r}\right)^n\right]$$
(A-2)

where x (nm) is the horizontal distance from the particle center, y (nm) is the particle height as a function of x, and n is a positive integer. Equation A-2 is defined for $0 \leq x \leq r$, and the 3-dimensional shape is obtained by revolving this function 2π radians about the y-axis. The volume, V_p (nm^3), and surface area, σ (nm^2), of an individual particle can be obtained by integrating Equation A-2, yielding Equations A-3 and A-4.

$$V_p = \frac{n\pi}{n+2}hr^2$$
(A-3)

$$\sigma = 2\pi \int_0^r x\sqrt{1 + \left(\frac{nh}{r^n}x^{n-1}\right)^2}\,dx$$
(A-4)

Equation A-4 is evaluated numerically. Note that for $n = 4$, Equation A-3 gives the volume of a half spheroid. The fitting parameter n was estimated by comparing volumes predicted by

59

Equation A-3 with the volume of individual AgNPs calculated by direct numerical integration of

deconvoluted AFM data, V_{AFM} (nm^3), where V_{AFM} was calculated by Equation A-5.

$$V_{AFM} = \sum A_i h_i \qquad \text{(A-5)}$$

where h_i (nm) is the measured height at pixel i, and A_i (nm^2) is the area of a single pixel. Pixels

were only included in the calculation if $h_i \geq 10$ nm. For the 300×300 nm images with 256×256

pixel resolution used for the integration, $A_i = 1.373$ nm^2. A comparison of V_{AFM} and V_p for

different values of the model parameter n is shown in Table A-1. The value that most frequently

gave the best fit was $n = 6$. In Figure A-1, a deconvoluted AFM image of an individual AgNP

and a modeled AgNP are shown.

Table A-1. Comparison of AgNP Volumes from Deconvoluted AFM Data and Equation A-3

Measured Height, h (nm)	Measured Radius, r (nm)	Volume from AFM Data, V_{AFM} (nm^3)	Predicted Volume from Equation A-3, V_p (nm^3)*				
			$n = 4$	$n = 5$	$n = 6$	$n = 7$	$n = 8$
58.6	48.3	3.16E+05	2.87E+05	3.07E+05	**3.23E+05**	3.34E+05	3.44E+05
69.1	43.3	3.09E+05	2.71E+05	2.90E+05	**3.05E+05**	3.16E+05	3.25E+05
61.7	42.8	2.62E+05	2.37E+05	2.53E+05	**2.66E+05**	2.76E+05	2.84E+05
60.9	40.0	2.05E+05	**2.04E+05**	2.18E+05	2.29E+05	2.37E+05	2.44E+05
52.5	46.2	2.49E+05	2.35E+05	**2.52E+05**	2.64E+05	2.74E+05	2.82E+05
57.6	38.1	1.97E+05	1.75E+05	1.88E+05	**1.97E+05**	2.04E+05	2.10E+05
53.0	42.3	2.31E+05	1.98E+05	2.12E+05	2.23E+05	**2.31E+05**	2.38E+05
66.4	48.3	3.59E+05	3.25E+05	3.48E+05	**3.65E+05**	3.79E+05	3.90E+05
69.9	41.6	2.74E+05	2.53E+05	**2.72E+05**	2.85E+05	2.96E+05	3.04E+05
58.9	38.6	2.18E+05	1.84E+05	1.97E+05	2.07E+05	**2.15E+05**	**2.21E+05**
53.6	38.7	1.88E+05	1.68E+05	1.80E+05	**1.89E+05**	1.96E+05	2.02E+05
53.2	45.6	2.72E+05	2.31E+05	2.48E+05	2.60E+05	**2.70E+05**	2.77E+05
54.8	39.8	2.00E+05	1.81E+05	1.94E+05	**2.04E+05**	2.12E+05	2.18E+05
46.8	39.3	1.78E+05	1.51E+05	1.62E+05	1.70E+05	**1.76E+05**	1.81E+05
49.3	39.4	1.89E+05	1.60E+05	1.71E+05	1.80E+05	**1.87E+05**	1.92E+05
46.1	33.2	1.16E+05	1.06E+05	**1.14E+05**	1.19E+05	1.24E+05	1.27E+05
46.9	32.0	1.14E+05	1.01E+05	1.08E+05	**1.13E+05**	1.17E+05	1.21E+05
41.5	32.0	1.02E+05	8.90E+04	9.54E+04	**1.00E+05**	**1.04E+05**	1.07E+05
44.6	32.8	1.16E+05	1.00E+05	1.08E+05	1.13E+05	**1.17E+05**	1.21E+05
39.4	34.3	1.18E+05	9.68E+04	1.04E+05	1.09E+05	1.13E+05	**1.16E+05**
40.7	32.5	1.05E+05	8.98E+04	9.62E+04	1.01E+05	**1.05E+05**	1.08E+05
37.2	32.4	9.56E+04	8.15E+04	8.74E+04	9.17E+04	**9.51E+04**	9.78E+04
38.7	35.4	1.21E+05	1.02E+05	1.09E+05	1.14E+05	1.19E+05	**1.22E+05**
51.0	40.7	2.01E+05	1.77E+05	1.89E+05	**1.99E+05**	2.06E+05	2.12E+05
36.1	31.2	9.01E+04	7.36E+04	7.89E+04	8.28E+04	8.59E+04	**8.83E+04**
39.3	30.2	8.43E+04	7.51E+04	8.04E+04	**8.44E+04**	8.76E+04	9.01E+04
32.5	27.5	5.89E+04	5.15E+04	5.52E+04	**5.79E+04**	6.01E+04	6.18E+04
27.9	24.9	4.34E+04	3.61E+04	3.87E+04	4.06E+04	4.21E+04	**4.33E+04**
30.6	23.0	3.98E+04	3.39E+04	3.63E+04	3.81E+04	**3.96E+04**	4.07E+04

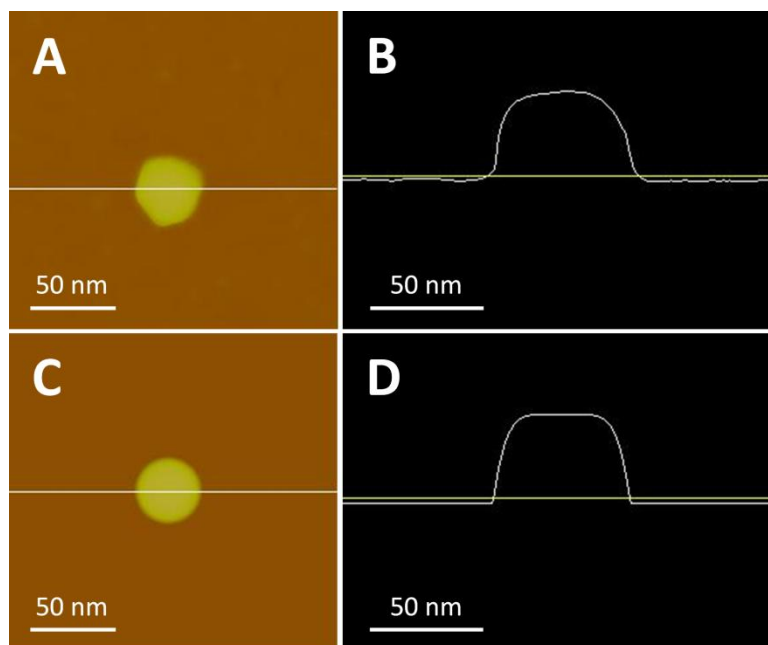*The value that most closely matches V_{AFM} is in bold and underlined.

Figure A-1. Deconvoluted AFM A) raster image and B) height profile for an AgNP after 14 d of dissolution in 300 mM NaCl. Modeled C) raster image and D) height profile of the AgNP shown in A) and B) using Equation A-2 with $n = 6$.

Appendix B: Aggregation

In Figure B-1, it is evident that aggregation of NSL-produced AgNPs occurred upon exposure to NaCl. Aggregation was observed to occur in as little as 2 h in 10 mM NaCl. The aggregation process cannot be explained entirely by classic DLVO theory because no aggregation was observed after 1 d of exposure to 10 mM $MgSO_4$. We also note that the aggregation almost exclusively involved the large irregular particles caused by defects in the latex colloid mask. Although mean AgNP height increased under the conditions shown in Figure B-1, aggregation does not appear to have played a role in this increase.
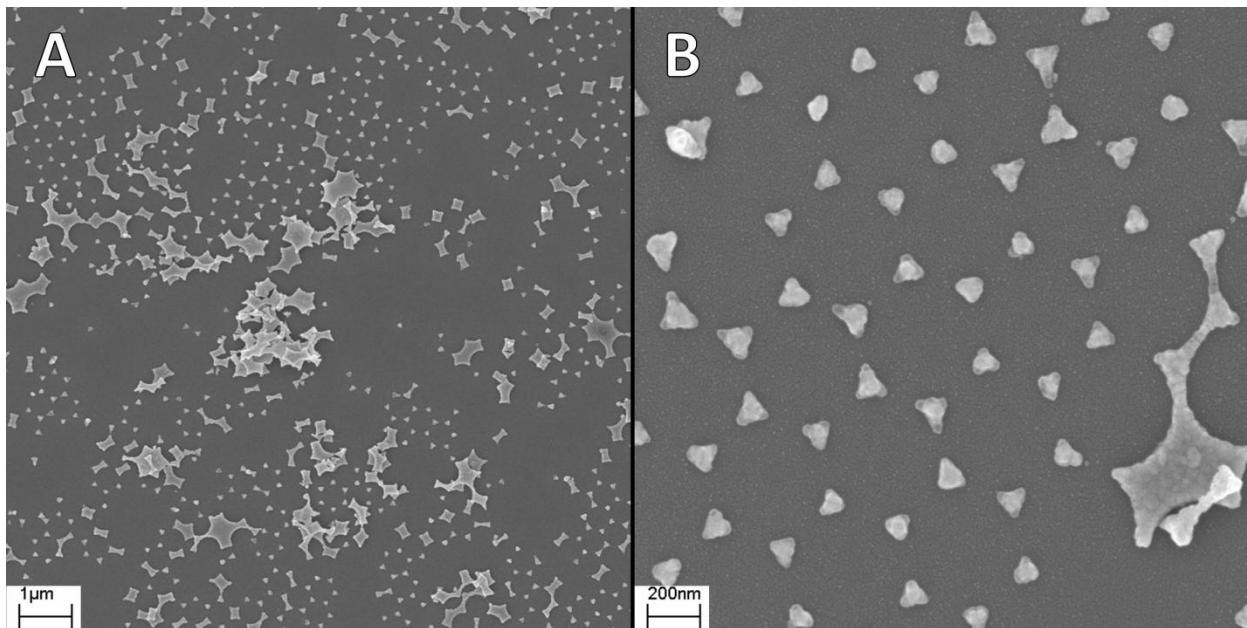
Figure B-1. SEM images of NSL-produced AgNPs after 9 d of exposure to 1 mM NaCl. A) Evidence of aggregation. B) High magnification image showing that the isolated regular particles used for the AFM analysis were apparently unaffected by the aggregation process. AFM measurements did indicate an increase in the mean particle height of these isolated regular AgNPs.

Appendix C: Dissolution Rates

Equation C-1 is based on AFM height measurements and gives the AgNP dissolution rate, R, in units of nm/d as a function of NaCl (mol/L).

$$R = 3.3029[NaCl] + 0.3563 \tag{C-1}$$

Dissolution rates, R_σ, in units of mg/m^2/d were calculated by Equation C-2.

$$R_\sigma = \frac{\Delta M}{\sigma_{ave} \Delta t} \tag{C-2}$$

where ΔM is the change in mass during the time interval Δt (d) and is calculated by multiplying Equation 3-3 by the solution volume, V_s (L), and converting from μg to mg. σ_{ave} is the average of the surface areas, calculated by Equation A-4 and converted to m^2, at the beginning and end of the time interval. R_σ is constant for a given NaCl concentration. Equation C-3 gives R_σ as a function of NaCl (mol/L).

$$R_\sigma = 33.932[NaCl] + 2.9705 \tag{C-3}$$

Appendix D: Predicted Concentrations

Regression equations for height and radius as a function of time (Figure 3-3) were used with Equations 3-2 and 3-3 to predict dissolved silver concentration as a function of time. Equation D-1 was fit to the predicted concentrations to obtain a pseudo-first-order kinetic model.

$$C = C_0(1 - e^{-kt}) \tag{D-1}$$

where C (μg/L) is the concentration at time t (d), C_0 (μg/L) is the concentration for complete dissolution, and k (d^{-1}) is the mass-based first-order rate constant. Fitting parameters for this model are given in Table D-1. C_0 decreased as the NaCl concentration increased because the intercepts of both the height and radius regression lines were higher, in general, at lower NaCl concentrations (Figure 3-3), which led to a larger initial particle volume predicted for the low concentrations. Plots of the predicted concentrations for a 4 mm^2 substrate are shown in Figure D-1.

Table D-1. Mass-based First-order Kinetic Parameters for AgNP Dissolution

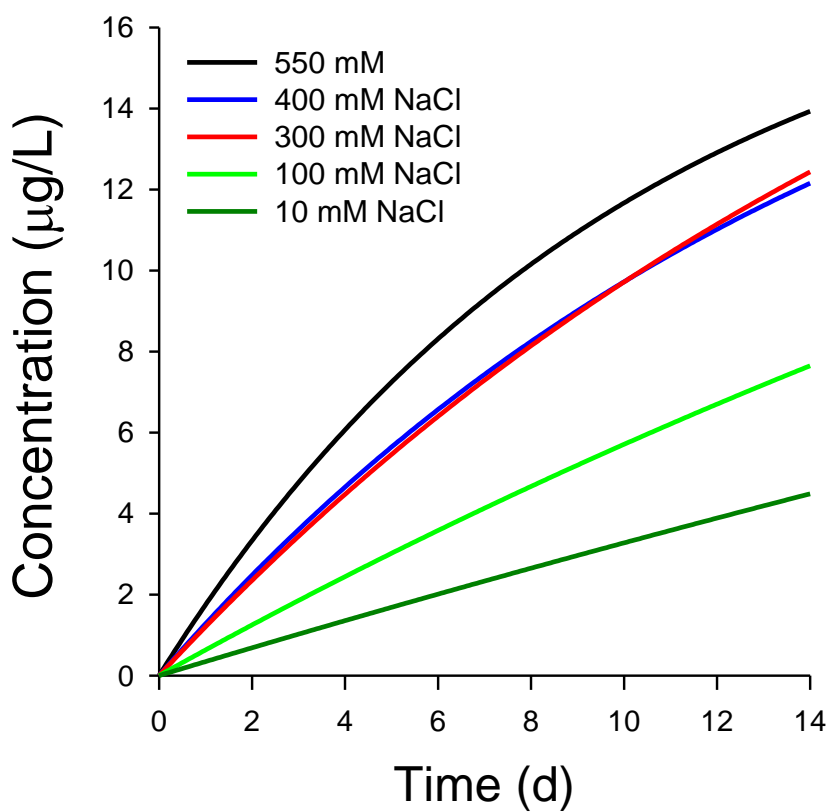| NaCl (mM)	k (d^{-1})	C$_0$ (μg/L)
10	0.0114	30.5044
100	0.0231	27.6638
300	0.0499	24.7305
400	0.0649	20.3630
550	0.0987	18.6029

Figure D-1. Modeled dissolved silver concentrations for a 4 mm^2 substrate.